Supplementary Information for

Balancing Europe's wind power output through spatial deployment informed by weather regimes

Christian M. Grams[1*], Remo Beerli[1], Stefan Pfenninger[2], Iain Staffell[3], and Heini Wernli[1]

[1]Institute for Atmospheric and Climate Science, ETH Zurich, Switzerland.
[2]Climate Policy Group, Institute for Environmental Decisions, ETH Zurich, Switzerland.
[3]Centre for Environmental Policy, Imperial College London, UK.

[*]Correspondence to: Christian Grams, Institute for Atmospheric and Climate Science, ETH Zurich, Universitätstrasse 16, 8092 Zurich, Switzerland, christian.grams@env.ethz.ch, +41 44 632 82 10.

This PDF file includes:

Other Supplementary Materials for this manuscript includes the following:

Supplementary Data 1 as zipped archive: WR_energy_CF_data.zip
- pv_DJF.txt
- pv_JJA.txt
- pv_MAM.txt
- pv_SON.txt
- wind_current_DJF.txt
- wind_current_JJA.txt
- wind_current_MAM.txt
- wind_current_SON.txt
- wind_nearterm_DJF.txt
- wind_nearterm_JJA.txt
- wind_nearterm_MAM.txt
- wind_nearterm_SON.txt
- wind_longterm_DJF.txt
- wind_longterm_JJA.txt
- wind_longterm_MAM.txt
- wind_longterm_SON.txt

Supplementary Discussion

1. Background on the seven Atlantic-European weather regimes

Here a meteorological perspective on the seven weather regimes is given based on 500 hPa geopotential height (*Z500*, Supplementary Fig. 1) and monthly weather regime frequencies (Supplementary Fig. 2). For comparison with other classifications[4,5,32] absolute values of *Z500* are shown for winter (DJF) without normalisation. Due to the annual definition (see Methods) the flow pattern is comparable in all seasons (not shown).

The "no regime" conditions are representative of the winter climatological mean (not shown) and exhibit no distinct anomalies in *Z500* (*Z500'*, shading in Supplementary Fig. 1h). The absolute *Z500* field (contours in Supplementary Fig. 1h) is characterised by a climatological trough over North America, and weak ridging over the eastern North Atlantic and western Europe. Strong westerly upper-level flow, parallel to the isohypses of geopotential height (contours in Supplementary Fig. 1h), prevails in the eastern and central North Atlantic, and reaches into Europe.

The seven weather regimes are deviations from these climatological mean conditions. We consider three of the seven weather regimes as cyclonic (AT, ZO, ScTr, Supplementary Fig. 1a-c) since the predominant signature is a negative *Z500* anomaly. The regimes ZO and ScTr are flanked by moderate positive *Z500* anomalies over Europe and the North Atlantic, respectively (Supplementary Fig. 1b-c). Four regimes are considered as blocked (AR, EuBL, ScBL, GL, Supplementary Fig. 1d-g) since their dominant feature is a strong positive *Z500* anomaly flanked by weaker negative anomalies.

The **Atlantic trough** regime (AT) features a single dominant negative *Z500* anomaly east of Ireland (Supplementary Fig. 1a). The upper-level flow is straight westerly between 40-50°N across the entire North Atlantic and into Europe (contours in Supplementary Fig. 1a). Due to the negative *Z500* anomaly located between Iceland and the Azores, the NAO index is positive (+0.40) during AT in winter (Supplementary Table 1).

The **Zonal regime** (ZO) is dominated by a negative *Z500* anomaly around Iceland and southern Greenland, and by weakly blocked conditions over western continental Europe due to an enhanced ridge (Supplementary Fig. 1b). It constitutes the actual positive phase of the NAO (NAO index +0.99 during ZO in winter, Supplementary Table 1). Compared to AT the negative anomaly is shifted poleward. Westerly upper-level flow prevails in the eastern North Atlantic and turns into southwesterly flow over the North Sea region and into Scandinavia (contours in Supplementary Fig. 1b).

During the **Scandinavian trough** regime (ScTr), the negative *Z500* anomaly is shifted eastward compared to ZO and a broad trough extends into northern and eastern Europe (Supplementary Fig. 1c). At the same time a positive *Z500* anomaly reflects weak ridging over the North Atlantic between 40-50°N. The prevailing upper-level westerly flow is shifted northward compared to AT (contours in Supplementary Fig. 1c). ScTr is NAO positive in winter (NAO index +0.88, Supplementary Table 1).

A strong positive *Z500* anomaly resides south of Iceland during the **Atlantic ridge** regime (AR) accompanied by a blocking ridge west of Ireland and a trough affecting wide parts of Europe (Supplementary Fig. 1d). The usually prevailing westerly flow is blocked and deflected around the ridge turning into northwesterlies over Northern and Western Europe (contours in Supplementary Fig. 1d). The NAO is weakly negative (–0.22, Supplementary Table 1).

During the **European blocking** regime (EuBL) a positive *Z500* anomaly is centred over the North Sea region and a blocking ridge expands over Western and Central Europe (Supplementary Fig. 1e). At the same time an upstream trough extends over the Labrador Sea and a downstream trough over Southeastern Europe (contours in Supplementary Fig. 1e). The upper-level flow is strongly deflected into southwesterlies from Newfoundland over Iceland to northern Scandinavia. This flow configuration projects weakly to the positive phase of the NAO in winter (+0.26, Supplementary Table 1).

During **Scandinavian blocking** (ScBL) the positive *Z500* anomaly is shifted into northern Scandinavia accompanied by a weaker negative anomaly in the eastern North Atlantic and Western Europe (Supplementary Fig. 1f). The upper-level flow is split with a branch deflected poleward around the blocking anticyclone and westerly flow over Iberia and the Mediterranean (contours in Supplementary Fig. 1f). The NAO index is weakly negative (–0.18, Supplementary Table 1).

Greenland blocking (GL) constitutes the negative phase of the NAO (mean NAO during GL in winter is –0.84, Supplementary Table 1). It features a strong positive *Z500* anomaly over Greenland and a zonally aligned negative anomaly stretching from the eastern North Atlantic into Northern Europe (Supplementary Fig. 1g). The prevailing westerly flow is deflected southward, centred around 40°N, and extends into the Mediterranean. Northern Europe is affected by northerly upper-level flow (contours in Supplementary Fig. 1g).

The mean NAO indices for the seven regimes show some seasonal variability (Supplementary Table 1). This is also due to the fact that the NAO index used here is based on the monthly varying leading EOF pattern; whereas our weather regime definition is based on year-round constant EOF patterns (see Methods).

From this overview of the seven weather regimes in winter and their mean NAO indices we conclude that the NAO alone does not account for the full range of large-scale flow variability in the Atlantic-European region and a mere interpretation of surface weather based on the NAO index would be misleading[19-21]. In contrast, our seven weather regimes reflect the seasonal variability of the preferred states of the large-scale midlatitude circulation in the Atlantic European region (Supplementary Fig. 2). All seven regimes share an equal annual frequency of 9 to 11% (right bar in Supplementary Fig. 2); while 31.5% of all days are attributed to no regime (grey in Supplementary Fig. 2, ranging from 20.7% in December to 41.7% in July).

In general, cyclonic regimes (AT, ZO, ScTr) are more frequent in winter months (November to March, Supplementary Fig. 2), in particular ZO. Summer months (May to September) are more frequently associated with blocked regimes (AR, EuBL, ScBL, GL, Supplementary Fig. 2), with a dominance of ScBL. Of the cyclonic regimes, AT occurs year-round, and is the preferred cyclonic regime in summer. In contrast, ZO and ScTr are more frequent in winter and in the transition seasons and almost absent in summer. Of the blocked regimes, GL occurs year-round. The two blocked regimes over Europe (EuBL and ScBL), albeit generally more frequent in summer, show opposite behaviour in relative seasonal preference. Whereas EuBL is the preferred blocking in Europe in core winter (EuBL 10.9% vs. ScBL 6.5%; Supplementary Fig. 2), ScBL occurs more frequently than EuBL in core summer (EuBL 12.2% vs. ScBL 16.0%, Supplementary Fig. 2). Finally, AR occurs more frequently in winter (9.7%) than summer (6.6%, Supplementary Fig. 2).

2. Seasonality of wind and solar PV generation in Europe

The seasonal evolution of renewable wind and solar PV power output aggregated for Europe is depicted in Supplementary Fig. 3 and Supplementary Table 3. The seasonal mean joint production of wind and solar PV (horizontal lines in Supplementary Fig. 3a-d,i-l, Supplementary Table 3) reaches 39.9 GW in winter (DJF), 41.0 GW in spring (MAM), 37.4 GW in summer (JJA), and 36.8 GW in autumn (SON).

Still, as detailed in the main text, seasonal mean wind generation is highest in winter (33.9 GW) and volatility in wind electricity generation, defined by the difference between the regime with maximum generation and minimum generation, culminates in winter at 22.4 GW (66% of winter mean generation; Supplementary Fig. 3a,e, Supplementary Table 3). Maximum mean wind generation occurs during the AT regime, minimum mean wind generation during EuBL. In contrast, in winter these regimes result in minimum and maximum mean solar PV generation, respectively. Thus volatility in solar PV generation is also high but an order of magnitude smaller compared to wind (1.9 GW, 32% of winter mean generation of 6.0 GW; Supplementary Fig. 3i,m, Supplementary Table 3). Because in winter wind generation and volatility are highest, and solar PV generation is lowest at high volatility, the main study focuses on this season.

In the transition seasons, spring and autumn, seasonal mean wind generation is lower (26.4 GW and 27.2 GW; Supplementary Fig. 3b,d; Supplementary Table 3; Supplementary Discussion 6). In addition, volatility is reduced in absolute terms (10.7 GW, 41% of spring mean wind generation and 15.6 GW, 57% of autumn mean wind generation; Supplementary Fig. 3b-h; Supplementary Table 3) but still affects a substantial fraction of seasonal mean generation. As in winter, EuBL is responsible for the severest underproduction. In summer, wind generation (20.0 GW) and volatility are low (6.9 GW) but volatility nevertheless reaches 34% of summer mean generation (Supplementary Fig. 3c,g, Supplementary Table 3); the most severe underproduction occurs likewise during EuBL in summer.

Solar PV generation behaves differently, with seasonal mean generation strongly increasing in spring (14.6 GW, Supplementary Fig. 3j, Supplementary Table 3), culminating in summer (17.3 GW, Supplementary Fig. 3k), and falling to 9.6 GW in autumn (Supplementary Fig. 3l). However, volatility remains at a much lower level compared to wind, culminating in spring at 2.6 GW (18% of spring mean generation, Supplementary Fig. 3n), having a minimum of 0.9 GW in summer (5% of summer mean generation, Supplementary Fig. 3o), and reaching 2.3 GW in autumn (23.8% of autumn mean generation, Supplementary Fig. 3p). In all seasons except summer overproduction from solar PV occurs during EuBL, underproduction during AT. However, their relative importance compared to other regimes has seasonal variations (Supplementary Fig. 3m-p, Supplementary Table 3).

Altogether our main conclusions about weather regime-dependent volatility in wind and solar PV electricity generation hold for all seasons, albeit at lower amplitude than in winter.

3. Seasonality in spatial patterns of wind, insolation, and temperature anomalies and their implications for the electricity system

The main text discussed the weather regime-dependent wind electricity generation patterns across Europe for winter (Fig. 1). Here the wind production potential during all seasons is presented (Supplementary Fig. 4) and regime-dependent variability in the 100 m wind speed during summer (JJA) is discussed (Supplementary Fig. 5), as well as the corresponding patterns for solar PV (Supplementary Figs. 6-8). We also include a brief discussion of 2 m temperature anomalies in winter and summer (Supplementary Figs. 9, 10) which potentially affect electricity demand[24] and

finish with a discussion of the implications of surface weather variability on the design of Europe's electricity system.

Wind

Three sub-regions with distinct potential for wind generation during different regimes and a gradual transition of this regime behaviour at their boundaries were identified for winter: Northern Europe with overproduction during cyclonic regimes (AT, ZO, ScTr), Southeastern Europe with overproduction during blocked regimes (AR, EuBL, ScBL, GL) culminating in EuBL, and the western Mediterranean with overproduction during AT, ScBL, and GL (discussion of Figs. 1, 2). These patterns hold also for the transition seasons spring and autumn (Supplementary Fig. 4b,d), albeit with a smaller amplitude of changes in wind generation potential.

Summer exhibits a slightly different behaviour (Supplementary Figs. 4c, 5). In general, winds across Europe are weaker in summer (contours and vectors in Supplementary Fig. 5h,i. cf. Fig. 2). Positive wind speed anomalies during the cyclonic regimes are confined to a smaller area and shift northward, affecting predominantly the North Sea region (Supplementary Fig. 5a-c cf. Fig. 2a-c). During ZO summer Etesians in the Aegean Sea are evident (Supplementary Fig. 5b) resulting in weak potential for overproduction in Greece and Bulgaria. However, ZO is rare in summer (3.5%, Supplementary Fig. 2, Supplementary Table 1). Prevailing northerly flow during AR results in weak potential for overproduction throughout continental Europe (Supplementary Fig. 5d). As in winter, wind generation potential is strongly reduced during EuBL and ScBL in the North Sea region but comparable to the seasonal mean in Southeastern Europe (Supplementary Fig. 5e,f). During GL weak cyclonic activity increases the potential for wind generation in Central and Eastern Europe and the western Mediterranean (Supplementary Fig. 5g).

Insolation

Throughout the year, the potential for solar PV generation during the different regimes anti-correlates with the potential for wind electricity generation (cf. Supplementary Figs. 4 and 6). As a measure for clear-sky conditions the local fraction of maximum potential solar insolation is indicated in Supplementary Fig. 6 (grey shading). Apparently, a strong North-South contrast exists, with the Mediterranean exhibiting values greater than 0.7 year-round, while a strong seasonal cycle is evident in Northern Europe (ranging from 0.2 in winter to 0.7 in summer). Consequently, weather regime-dependent changes in solar PV generation are weak in Southern Europe and summer, and more important in Central and Northern Europe during winter and the transition seasons. Here, large-scale subsidence during blocked regimes (AR, EuBL, ScBL) results in more insolation (Supplementary Figs. 7d-f) and a strong increase of the solar PV generation potential by up to 40% in winter (Supplementary Fig. 6a). During summer the amplitude of changes in insolation is much weaker and affects smaller areas (cf. Supplementary Figs. 7 and 8). Still, it is noteworthy that during the rare summer ZO regime enhanced high pressure in Eastern Europe increases Europe-wide solar PV power output (inset Supplementary Fig. 6c, Supplementary Fig. 8b). However, variability in spring and summer solar PV generation, when seasonal mean generation is highest, is much smaller (Supplementary Fig. 6b,c, Supplementary Table 3), corroborating that weather regime-dependent volatility in solar PV generation is less relevant than for wind electricity generation. For completeness, the data is shown without further discussion.

Temperature

Amongst factors affecting electricity demand, ambient air temperature is particularly important[24]. In summer, high temperatures increase the demand for air conditioning and other cooling technologies, while in winter, low temperatures increase the demand for heating and lighting. Long-lasting periods of low (high) temperature in winter (summer) can thus be used as a proxy for higher demand. As electric heating (cooling) is increasingly deployed in Europe, the increase in demand associated with cold (hot) weather will become even stronger[42].

In winter (Supplementary Fig. 9) cyclonic regimes generally go along with mild conditions due to the advection of mild oceanic air into the continent (AT, ZO, ScTr, Supplementary Fig. 9a-c). Whereas mild conditions prevail in entire Europe for AT, they are enhanced but focused more on Central, Northern, and Eastern Europe during ZO, and Northeastern Europe during ScTr. In contrast, blocked regimes are accompanied by cool conditions (Supplementary Fig. 9d-g). During the AR regime northwesterly flow into the continent and high pressure in Western Europe result in cool conditions throughout continental Europe. During EuBL this focusses more on Central and Southeastern Europe, with strong northerly flow in the Balkans, leading to very cool conditions and strong near-surface wind (Supplementary Fig. 9e). Concomitant cyclonic activity in Northern Europe causes mild conditions in northern Scandinavia. The coldest conditions occur during ScBL (in Eastern and Central Europe) and GL (in Northern and Central Europe).

In summer (Supplementary Fig. 10) the behaviour of temperature is opposite to winter. Cyclonic activity goes along with cooler conditions, whereas regions of high pressure are associated with warm conditions. During AT and ZO low pressure systems over the Atlantic cause rather cool conditions in the North Sea region and Scandinavia. However, the tendency for concomitant high pressure in the Balkans (AT) and Central Europe (ZO) also result in warmer conditions than the seasonal mean there. Northwesterly flow from the Atlantic during ScTr and AR encompasses most parts of Europe and leads to cool conditions. During EuBL and ScBL high pressure over Europe results in very warm conditions in most parts of Europe.

Implications for the electricity system

The discussion of 100 m wind, insolation, and 2 m temperature anomalies revealed important multi-day variability in surface weather modulated by weather regimes. In winter, low pressure mostly goes along with high wind speeds, low insolation, but mild conditions. This implies potential for high wind power output, reduced solar PV output and lower demand. Contrary, high pressure mostly goes along with strongly reduced surface wind, enhanced insolation, and cold conditions. This implies low wind power, high solar power (albeit relative to the low potential in winter) and high demand.

Therefore one could argue that co-deployment[12-14,19,44-47] of wind and solar PV could alleviate these variations. However, solar PV output in winter is strongly reduced due to seasonality (see Supplementary Discussion 2). It has been shown that co-deployment of wind and solar PV can balance *seasonal* variations in wind and solar PV[13] (wind power output is lower in summer, while solar PV is higher and vice-versa). But in order to mitigate also the *multi-day* volatility in wind generation and the shortfall during the critical blocked regimes in winter it would be required to massively expand its capacity compared to the current system. At the same time these shortfalls on the multi-day timescale occur during periods of potentially high electricity demand. Therefore we conclude that the suggested balancing by exploiting concomitant high wind generation potential in peripheral regions of Europe could be a meaningful strategy to address the *multi-day volatility* challenge imposed by weather regimes.

Our analyses provide an in-depth meteorological understanding of multi-day volatility in wind and solar PV generation based on country-aggregated generation. We then demonstrated how deployment strategies based on this novel insight could effectively exploit weather regime-dependent continent-scale wind conditions to balance Europe-wide wind generation.

For an optimally balanced electricity system also other renewables such as hydropower, tidal or biomass power need to be considered. In addition to production, also energy storage, transmission, demand, and an overall cost analysis is needed[15,25,26,48]. The feasibility of our balanced scenario for wind should therefore be explored with such a comprehensive approach in future work. This effort should go along with an investigation of optimal sites within a country[44,47]. Recently it was shown[42,47] that wind generation within a country can be optimised by exploiting local variations in wind conditions and that less sensitivity of country-aggregated solar PV output on specific sites exists than for wind[47]. Our analysis of multi-day surface weather variability (Fig. 2, Supplementary Figs. 5, 7-10) shows that some larger countries such as France, Norway or Sweden span regions with different multi-day wind variability. For instance, Northern Norway and Sweden experience higher winds during EuBL and ScBL than the southern part of these countries (Fig. 2e,f). Likewise regional wind systems such as the Mistral in southern France, the Bora in the Adriatic Sea, and the Etesians in the Aegean Sea impose multi-day variability on sub-country level, which requires more sophisticated strategies for optimal site selection

Still we note that, in reality, the deployment of technologies most likely does not follow such optimal trajectories. In addition, it is difficult to predict how energy policies across Europe will develop and be implemented over the coming decades. Thus, it is important also to consider how just one technology – here wind generation – can, through exploiting an improved meteorological understanding of multi-day weather patterns, provide a more stable power supply irrespective of how the rest of the European power system develops.

4. Discussion of future wind sites

The main text discussed the future "2030 Planned" scenario consisting of the build-out of the current planning pipeline until 2030, and the "2030 Balanced" scenario with new capacity deployed in peripheral regions of Europe. Supplementary Table 2 summarises characteristics of all scenarios investigated in this study. The "2030 Planned" and "2030 Balanced" scenarios are conservative in the sense that they are based on constant current *CF*s assuming the same technology and site characteristics as of 2015. However, it is expected that CFs increase by a third until 2030 due to an increase in offshore deployment and technical innovation[23].

Supplementary Fig. 11a shows the location of current wind farms ("historic", grey), wind farms being installed in the next few years ("near-term", blue), and wind farms in planning with anticipated deployment by 2030 ("long-term", red) from Staffell and Pfenninger[23]. It is obvious that while historic sites are more evenly distributed on shore and within each country, future deployment is focussed massively on coastal regions, with a predominance in the North Sea.

Renewables.ninja[23] provides national aggregate *CF*s for these future wind sites which we can use to compute future total wind production in Europe according to current planning and accounting for a shift in sites and advanced technology (Supplementary Discussion 5, Table 4, Fig. 12). However, these *CF*s are limited in their use for constructing an alternate balanced scenario. This is because of their geographical bias towards coastal regions and/or only little information about very few future sites (e.g. in Portugal, Italy, Greece, the Balkans, or Norway) the representativeness for the entire country is diluted. To illustrate that we show country-specific relative change in wind electricity generation for winter ($\Delta CF_{wr,country\ DJF}$) as in Fig. 1 but based on only the future *CF*s for newly installed capacity in construction (Supplementary Fig. 11c, "near-term" sites) or in planning (Supplementary Fig. 11d, "long-term" sites). Here the

underlying meteorological conditions are the same for each scenario, so that differences between them are solely due to an imbalance of new technology within countries that belong to different climatological sub-regions or for which only information about very few future sites are present. Whereas $\Delta CF_{wr,country\ DJF}$ shows only little changes in countries adjacent to the North and Baltic Seas that plan to massively expand their installed capacity, stronger changes of $\Delta CF_{wr,country\ DJF}$ are evident in countries with only few future sites e.g. Norway. Here information about a single site in the South is available which exhibits the inter-regime behaviour typical for the North Sea region with potential for strong underproduction during EuBL (Supplementary Fig. 11c,d, Fig. 2e). However, current sites are also located in northern Norway (Supplementary Fig. 11a) and yield an overall weak overproduction during EuBL (Supplementary Fig. 11b) due to enhanced wind during EuBL in northern Scandinavia (Fig. 2e). Other countries spanning diverse climatological sub-regions are France or Sweden. Thus future planning needs to consider weather-regime dependent wind patterns within a country in order to fully exploit their wind electricity potential[42,47].

For the reasons discussed above we have used the more conservative future scenarios based on the current *CF*s in the main text. Supplementary Discussion 5 shows that our key findings are not altered by a different setup.

5. Future scenarios for wind generation and their seasonality

The main text showed results for winter only. Here we discuss mean generation and volatility in the other seasons for the "2030 Planned" and "2030 Balanced" scenarios of the main text (Supplementary Tables 4, 5, Supplementary Fig. 12i-p). In addition mean generation for a future "2030 Planned fCF" scenario using future CFs for new wind sites (Supplementary Table 4, Supplementary Fig. 12a-h) and a simplified, but feasible "2030 Balanced simple" scenario are presented (Supplementary Table 6).

In the future "2030 Planned" scenario based on constant *CF*s, volatility in mean generation from regime to regime ranges from 52 GW in winter to 19 GW in summer, a relative fraction of 66% to 42% of the seasonal mean generation (Supplementary Table 4, Supplementary Fig. 12i-l). In all seasons minimum mean generation occurs during EuBL, while maximum generation occurs during AT or ScTr. In the "2030 Balanced" scenario with new wind farms deployed in Iberia, the Balkans, and northern Scandinavia (Supplementary Table 5, Supplementary Fig. 12m-p), this regime-dependent volatility is strongly reduced, in particular in winter. It ranges from 16 GW in spring to 13 GW in summer equivalent to a share of 27% and 20% of seasonal mean generation. Albeit volatility becomes relatively high in spring this stems rather from an overproduction in the ScTr regime (+9.3 GW, Supplementary Table 5). Seasonal mean generation in all seasons but winter is higher in the balanced scenario, compared to the planned scenario.

One might argue that the Balkans and northern Scandinavia (Norway and Finland) currently only have limited installed wind capacity, therefore current *CF*s were not representative for these countries, and future *CF*s should be used instead. However, we only have limited information about future *CF*s in Europe's peripheral regions (Supplementary Fig. 11a, Discussion 4). Therefore we explore a simplified balanced scenario ("2030 Balanced simple", Supplementary Table 6) with new deployment only in Portugal (few future deployments considered to be representative for entire country), Finland (new deployment planned at several sites across the entire country), and Greece (several new sites in the Aegean Sea). Overall results for this scenario based on current *CF*s (Supplementary Table 6, top) hardly differ from the original "2030 Balanced" scenario with spreading new capacity over several countries in each peripheral region (Supplementary Table 5). However, a caveat of new deployment in only a few countries is strongly enhanced intra-regime volatility at the short timescale (not shown) which is reduced with

more widespread deployment in Europe's peripheral regions as in the "2030 Balanced" scenario (Fig. 5, Supplementary Discussion 6).

With future *CF*s mean generation in the "2030 Balanced simple fCF" scenario increases by 20-30% and reaches 97 GW in winter. Still volatility levels remain moderate ranging from 14 GW in winter to 29 GW in summer, a share of 14% and 29% of seasonal mean generation respectively (Supplementary Table 6, bottom). In the future scenario based on future *CF*s and following actual planning ("2030 Planned fCF") mean generation levels are similar, but volatility is much higher (Supplementary Table 4, bottom, Supplementary Fig. 12a-h). It ranges from 61 GW in winter to 24 GW in summer, a share of 62% and 41% of seasonal mean generation respectively. Thus also scenarios which account for more efficient turbines and off-shore sites corroborate our findings based on the more conservative assumption of constant *CF*s.

In the main text, we showed that investment in peripheral regions of Europe would effectively exploit the geographical smoothing effect of weather regime-dependent wind electricity generation patterns and balance weather-regime dependent mean generation levels overall. Summarising the discussion above, these results hold for all seasons, and for two additional scenarios: (1) assuming future *CF* accounting for technology- and location-driven *CF* increases rather than conservative constant *CF*, and (2) focussing new capacity on only one country in each peripheral region.

6. Intra-annual volatility in wind production on seasonal, multi-day, and short-term timescales and its modulation by weather regimes

Overview

Our study showed that weather regimes explain a large fraction of *multi-day* variability (several days to a few weeks) in wind electricity generation. Other important intra-annual variations occur on *short-term* (hours to days) and *seasonal* (several months) timescales.

Supplementary Fig. 13 summarises intra-annual variability on these three distinct scales. The seasonal stratification (groups in Supplementary Fig. 13) reveals seasonal variability with roughly 50% higher wind power output in winter than in summer (or summer production reaching roughly 2/3 of winter production, cf. Supplementary Tables 3-5). In the "2030 Balanced" scenario (green in Supplementary Fig. 13) summer power output is slightly higher than in the "2030 Planned" scenario (orange in Supplementary Fig. 13), suggesting that the deployment in peripheral regions also dampens seasonal variability in wind power output.

The 5-day moving average removes short-term variability and reflects multi-day variability imposed by weather regimes (Supplementary Fig. 13b). As discussed for winter in the Main text (Fig. 5b), the balanced deployment (green, Supplementary Fig. 13b) strongly reduces multi-day variability to a level already known in the current system (black, Supplementary Fig. 13b) – but at overall higher power output. This generally holds for all seasons.

The larger variability for the six-hourly time series (Supplementary Fig. 13a) reflects short-term fluctuations that remain for all seasons but are easier to address with storage and flexible demand[15].

It is striking that in all seasons the lower 5th percentile for the six-hourly time series is about 7 GW to 12 GW higher in the "2030 Balanced" scenario (ranging from 30 GW to 48 GW) than in the "2030 Planned" scenario (ranging from 21 GW to 35 GW, Supplementary Fig. 13a). This suggests that the deployment in peripheral regions also provides a higher fleet-wide minimum output from wind energy.

Intra-regime volatility

For simplicity in the main text we primarily discussed multi-day volatility with weather regime-dependent *mean generation* in winter and showed that it can be substantially reduced by deployment strategies that account for geographical wind patterns. In the following we want to explore this issue for all seasons, using the full continuous six-hourly production time series (Supplementary Fig. 14, cf. Fig. 5 for winter).

It is evident that in the current system (Supplementary Fig. 14a,d,g,j). relatively high variability exists between the regimes in winter, spring, and autumn. Cyclonic regimes (AT, ZO, ScTr) overall exhibit higher production levels than blocked regimes (AR, EuBL, ScBL, GL). Time periods falling into EuBL generally exhibit very low production levels (75^{th} percentile < 30 GW for all seasons. In addition relatively high intra-regime volatility (cf. inter-quartile ranges) exists.

This behaviour will strongly amplify if deployment follows current planning (Supplementary Fig. 14b,e,h,k) and overall production levels in summer remain low. However, deployment in Europe's peripheral region and interconnection would not only yield a more balanced mean wind electricity generation between different regimes, but also strongly reduce intra-regime variability (Supplementary Fig. 14c,f,i,l). In addition the fleet-wide minimum output provided by wind power tends to remain at a much higher level, as reflected in the lower 5^{th} percentile. In winter this remains above 40 GW for all regimes, falling to around 30 GW in summer (Supplementary Fig. 14c,i). In the "2030 planned" scenario the lull in the North Sea during EuBL lowers the fleet-wide minimum output by about 10 GW throughout all seasons compared to the balanced scenario.

Thus deployment strategies informed by weather regimes could not only minimise differences in mean generation levels for the different weather regimes but also reduce intra-regime volatility and, most importantly, increase the fleet-wide minimum output provided by Europe's wind fleet.

We finally corroborate the validity of this statement across all seasons by showing the frequency distribution of wind *CF* (Supplementary Fig. 15) as discussed in the Main text for winter (Fig. 5c-e). In all seasons the histograms for the balanced scenario reflect only the remaining normally-distributed short-term fluctuations that are similar for all regimes (Supplementary Fig. 15 right column). In contrast, in all seasons, the seasonal mean frequency distributions for the current and planned scenario (black in Supplementary Fig. 15 left, middle) are skewed to low *CF*s with a long tail towards high *CF*s due to Europe-wide low *CF*s in blocked regimes (dashed in Supplementary Fig. 15 left, middle) and higher *CF*s in cyclonic regimes (solid in Supplementary Fig. 15 left, middle).

7. Verification with operator data

For a limited number of countries *CF* for wind and PV based on transmission system operator (TSO) power output data[39-41] is available for recent years (see Methods and Supplementary Table 7). The common data period is 1.1.2011-30.5.2016 for wind and 1.1.2012-30.5.2016 for PV. We verify the regime attribution based on Renewables.ninja data against TSO data in these shorter sub-periods (Supplementary Figs. 16-19). It has to be noted that winters (DJF) in these years were strongly governed by cyclonic regimes so that the interpretation for winter blocked regimes is limited (cf. bar width in Supplementary Fig. 3 and Supplementary Fig. 16). In contrast, summers (JJA) in these years were strongly governed by the blocked EuBL, ScBL, GL regimes so that only limited interpretation for summer cyclonic and AR regimes is possible. These differences in regime frequencies compared to the entire data period (1979-2015, Supplementary Fig. 2, Supplementary Table 1) reflect inter-annual variability in weather regime occurrence.

For wind, *CF* derived from the independent datasets is almost identical to Renewables.ninja data for both winter and summer (Supplementary Figs. 16, 17). In particular our key findings of strong overproduction in Germany and Great Britain during cyclonic regimes, and concurrent meteorological potential for overproduction in Greece and underproduction in the North Sea region (Germany, Great Britain) during EuBL holds despite the limited data coverage. Also the weather regime-dependent variations of *CF* in winter during the sufficiently frequent AT, ZO, ScTr, and ScBL regimes are comparable to the behaviour in the longer 1985-2016 reference period (cf. Supplementary Fig. 16, Fig. 3).

For solar PV there is a slightly different picture (Supplementary Figs. 18, 19). Solar power output is strongly sensitive to cloud cover and thus depends on a correct depiction of cloud cover in the reanalysis data. However, it is known that MERRA-2 has deficits in correctly depicting cloud coverage, in particular during high-pressure conditions in winter[22].

Regime-dependent solar PV *CF* based on TSO and Renewables.ninja data are almost identical for the cyclonic regimes (Supplementary Figs. 18, 19). The TSO-reported data indicates lower *CF*s during blocked regimes in winter than Renewables.ninja (Supplementary Fig. 18) causing even weak underproduction during blocked conditions in some countries. A potential meteorological explanation is the frequent occurrence of low stratus clouds (fog) during high-pressure conditions in winter, which models have difficulties to represent. However, our main finding that solar PV is much less affected by weather regime-dependent volatility than wind is confirmed despite the limited data coverage and potential limitations in cloud representation in MERRA-2.

Additional References for Supplementary Discussions

44. Jerez, S., Trigo, R. M., Sarsa, A., Lorente-Plazas, R., Pozo-Vázquez, D., & Montávez, J. P. Spatio-temporal complementarity between solar and wind power in the Iberian Peninsula. *Energy Procedia*, **40**, 48-57 (2013).

45. Santos-Alamillos, F. J., Pozo-Vázquez, D., Ruiz-Arias, J. A., Lara-Fanego, V., & Tovar-Pescador, J. Analysis of spatiotemporal balancing between wind and solar energy resources in the southern Iberian Peninsula. *J. Appl. Meteor. Climatol.*, **51(11)**, 2005-2024 (2012).

46. Nema, P., Nema, R. K., & Rangnekar, S. A current and future state of art development of hybrid energy system using wind and PV-solar: A review. *Renewable and Sustainable Energy Reviews*, **13(8)**, 2096-2103 (2009).

47. Jerez, S., Thais, F., Tobin, I., Wild, M., Colette, A., Yiou, P., & Vautard, R. The CLIMIX model: A tool to create and evaluate spatially-resolved scenarios of photovoltaic and wind power development. *Renewable and Sustainable Energy Reviews*, **42**, 1-15 (2015).

48. MacDonald, A. E. *et al.* Future cost-competitive electricity systems and their impact on US CO2 emissions. *Nature Clim. Change* **6,** 526–531 (2016).

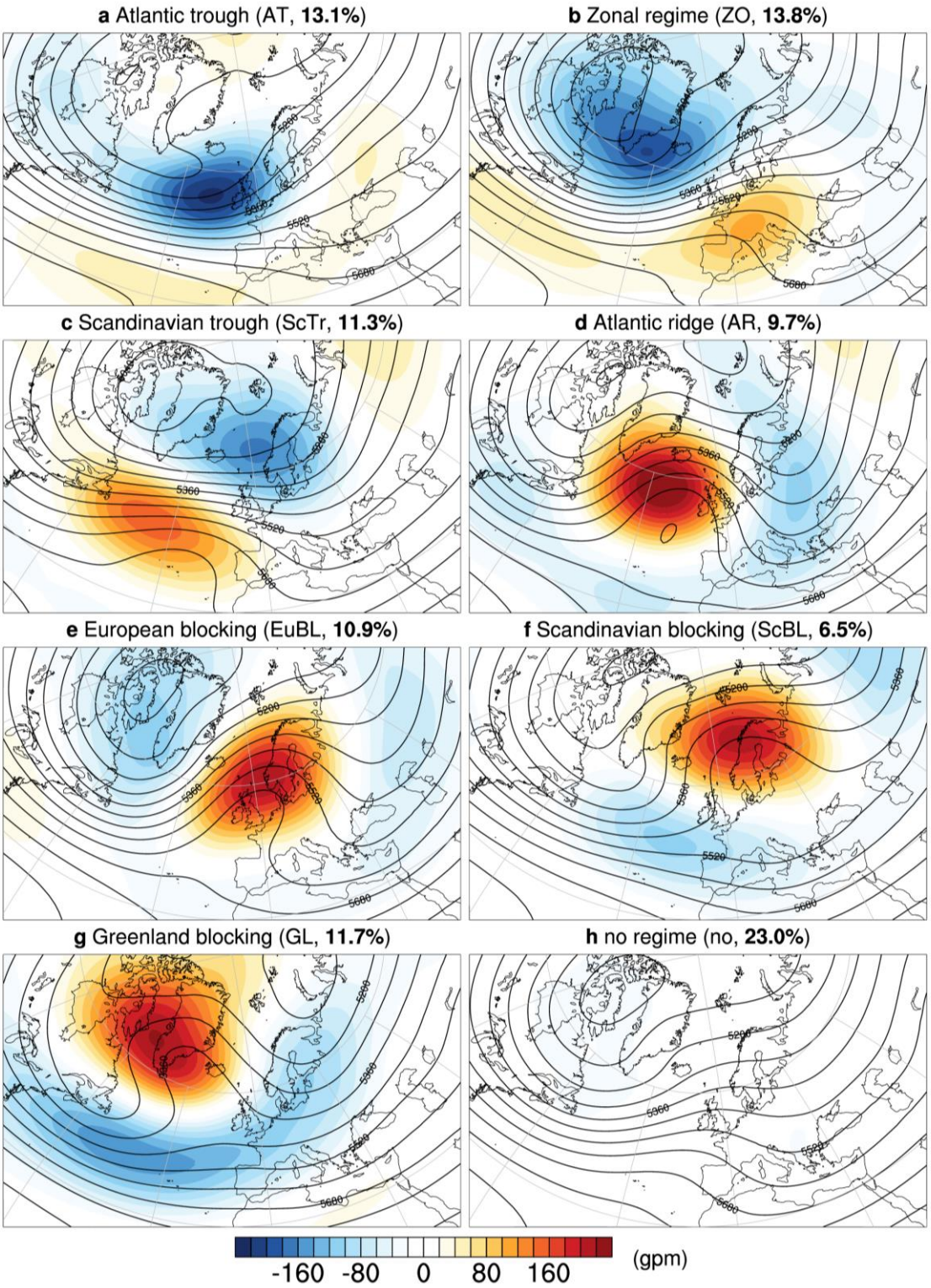

Supplementary Figure 1. Atlantic-European weather regimes in winter.

Mean low-pass filtered (10 days) 500 hPa geopotential height anomaly (*Z500'*, shading, every 20 geopotential meters), and mean absolute 500 hPa geopotential height (*Z500*, black contours, every 40 geopotential meters) in winter (DJF) for all days attributed to one of the 7 weather regimes (a-g) and to no regime (h). Although the regime definition is based on normalised data for the entire year, here non-normalised data for DJF are shown. Regime name, abbreviation, and relative frequency (for winter, in percent) indicated in the sub-figure caption.

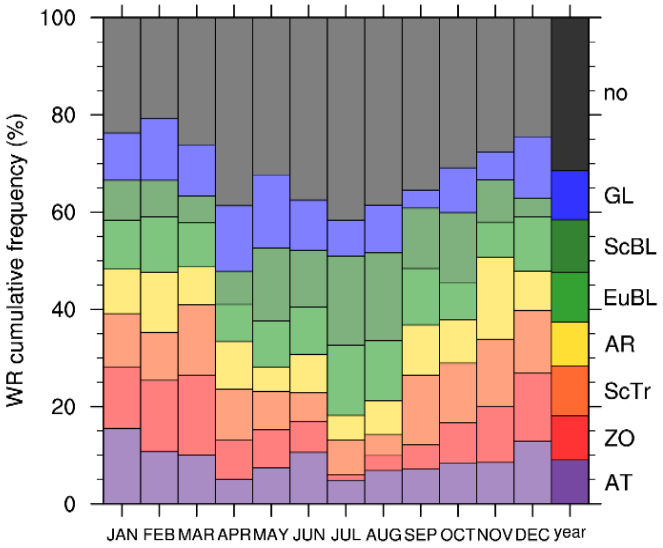

Supplementary Figure 2. Relative frequencies of the 7 weather regimes.

Cumulative relative frequency (in percent) of days classified into one of the seven regimes or no regime for each month during 1979-2015 (light colours) and the entire year (dark colours, last column). Regime abbreviations on the right.

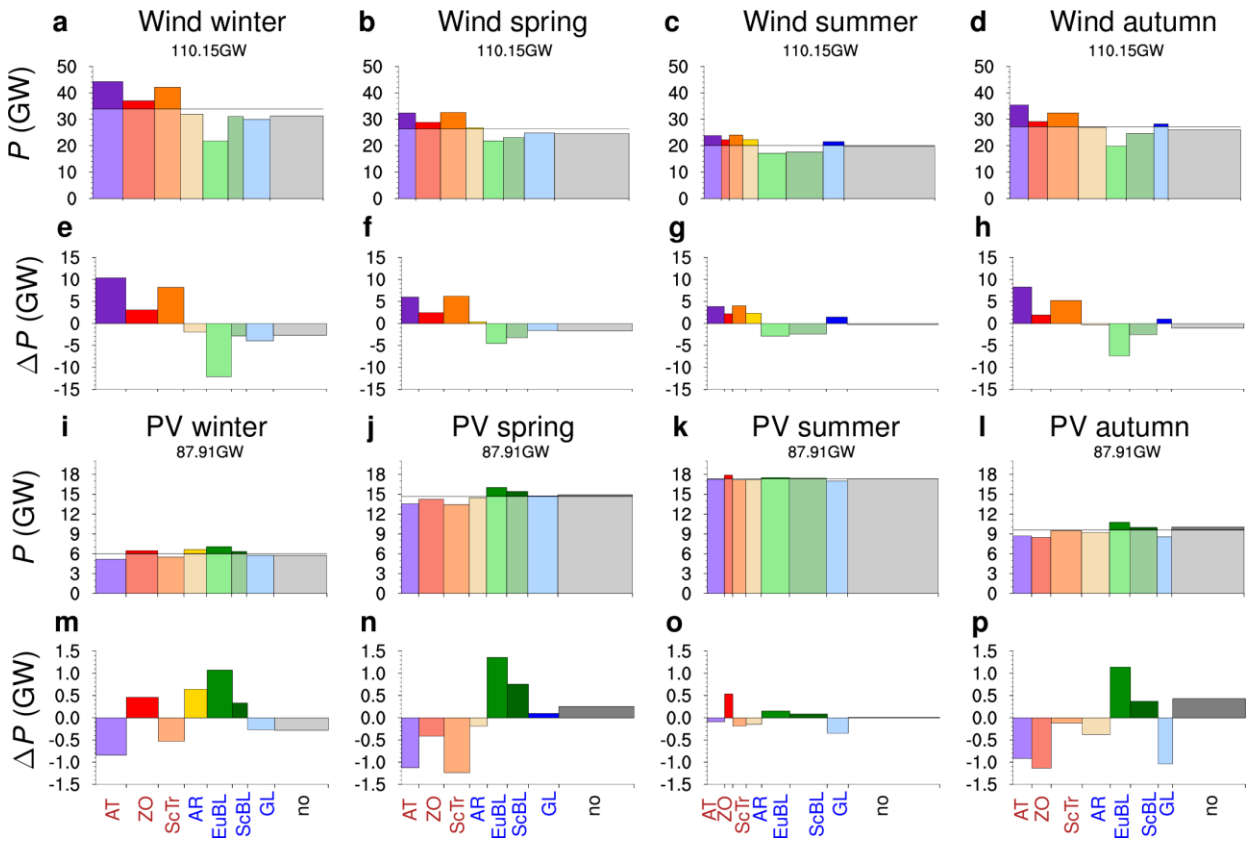

Supplementary Figure 3. Weather regime-dependent wind and solar PV power output.

Absolute electricity generation (*P* in GW) from wind (a-d) and solar PV (i-l) as in Fig. 3e, for all days from 1985-2016 classified into the seven weather regimes (coloured bars, red labels cyclonic, blue labels blocked), and no regime (grey, last bar). Dark colours highlight portion of bar above whole winter mean (horizontal line). Installed capacity as of 2015 indicated. (e-h, m-p) show absolute difference in wind and solar PV generation with respect to the seasonal mean as in Fig. 4d. Bar widths are scaled with seasonal occurrence frequency of the respective regime. Each column corresponds to a season (winter: DJF, spring: MAM, summer: JJA, autumn: SON). Note the different scale of the y-axis for wind and solar PV.

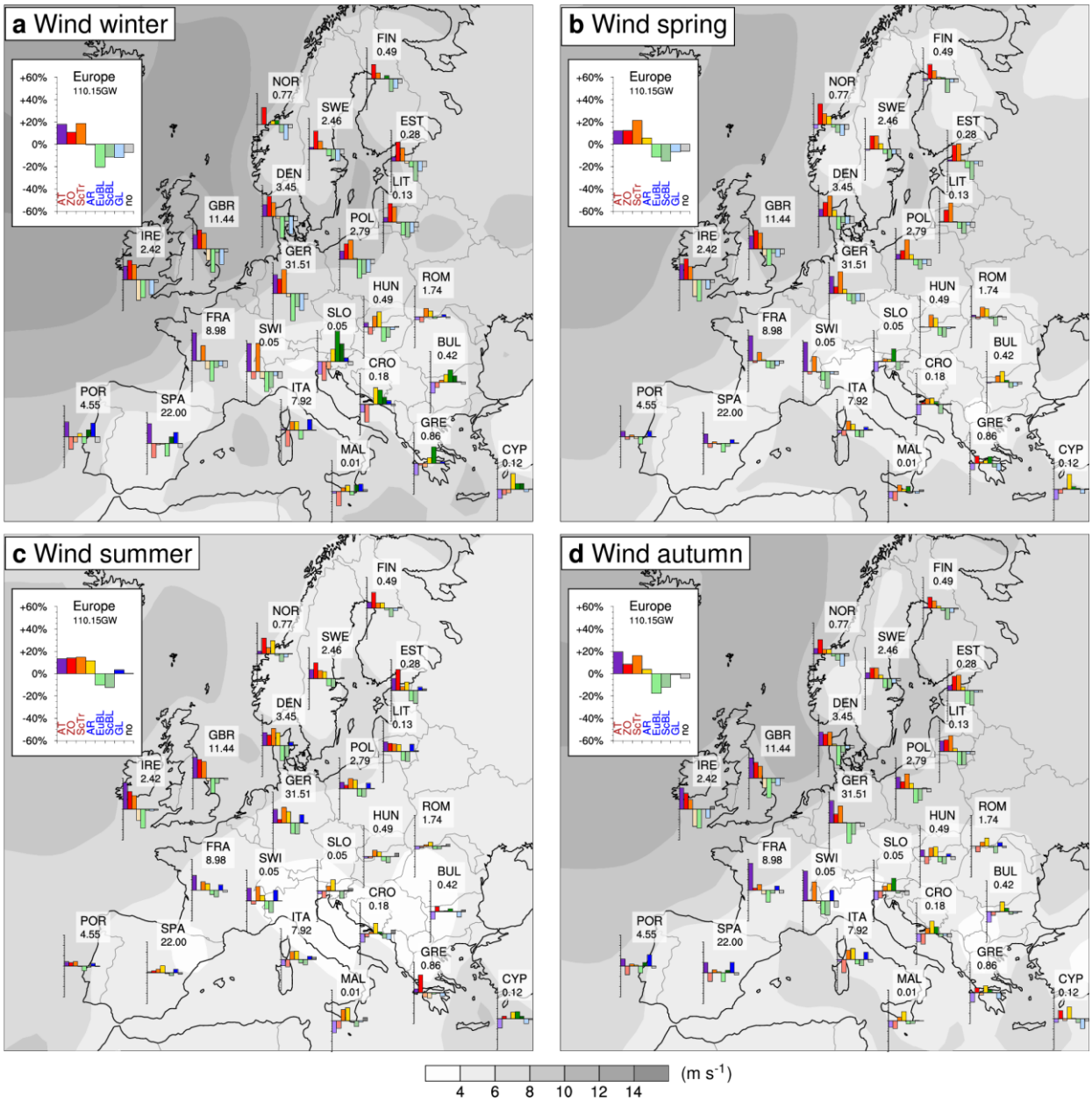

Supplementary Figure 4. Weather regime-dependent relative change in wind power output.

As Fig. 1 but for all seasons. Country-specific relative change in mean wind electricity generation during cyclonic (red labels, inset) and blocked regimes (blue labels), and no regime days (grey) normalised against seasonal mean generation (dark colours overproduction, light underproduction). Labels above barplots indicate three-letter country ISO code and installed capacity (in GW, as of 2015). Grey shading on map shows seasonal mean (1979-2015) 100 m wind speed (m s^{-1}). See inset for entire Europe and axis labels.

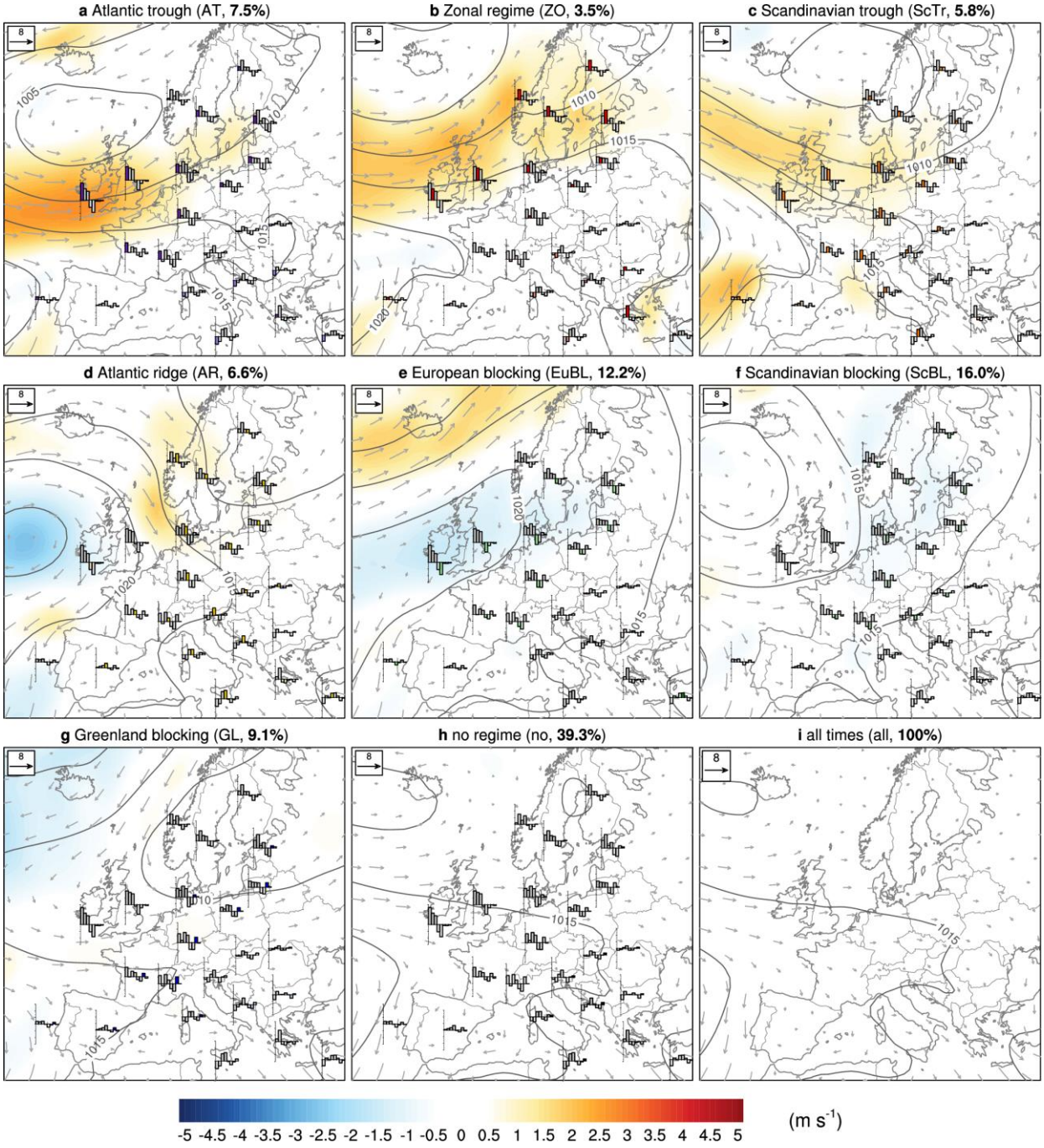

Supplementary Figure 5. Wind anomalies during the weather regimes in summer.

As Fig. 2, 100 m wind speed anomalies (blue-red shading in m s^{-1}), absolute wind at about 100 m (grey vectors), and mean sea level pressure (contours every 5 hPa) but for summer (JJA) days during each regime (a-g), no regime (h), and whole summer (i). Country-specific barplots from Supplementary Fig. 4c, with respective regime coloured. Frequency of weather regimes (%) in panel captions.

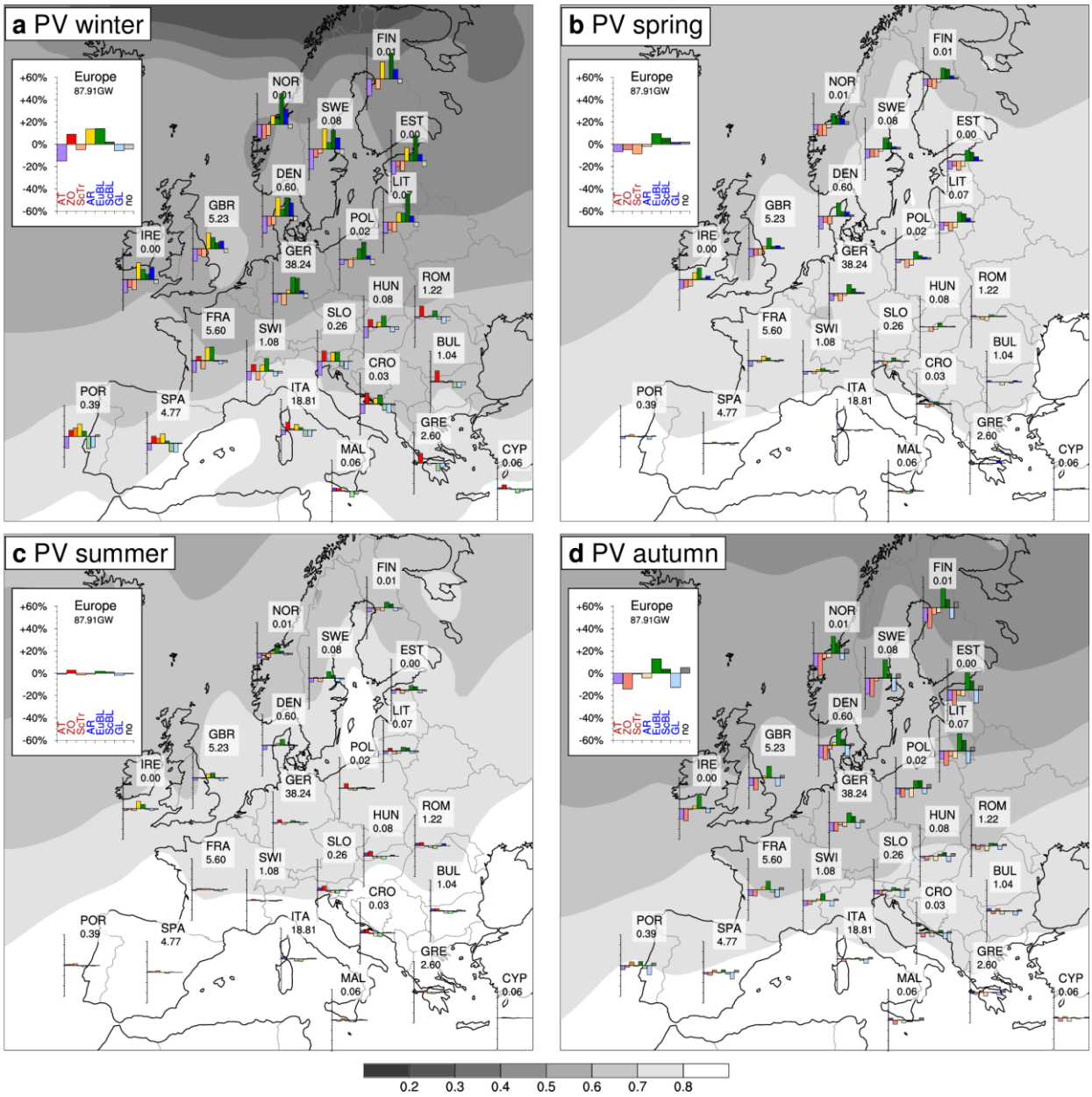

Supplementary Figure 6. Weather regime-dependent relative change in solar PV power output.

As Supplementary Fig. 4 but for solar PV electricity generation. The grey shading on the map shows seasonal mean (1979-2015) of the daily fraction of insolation and daily potential insolation assuming clear skies.

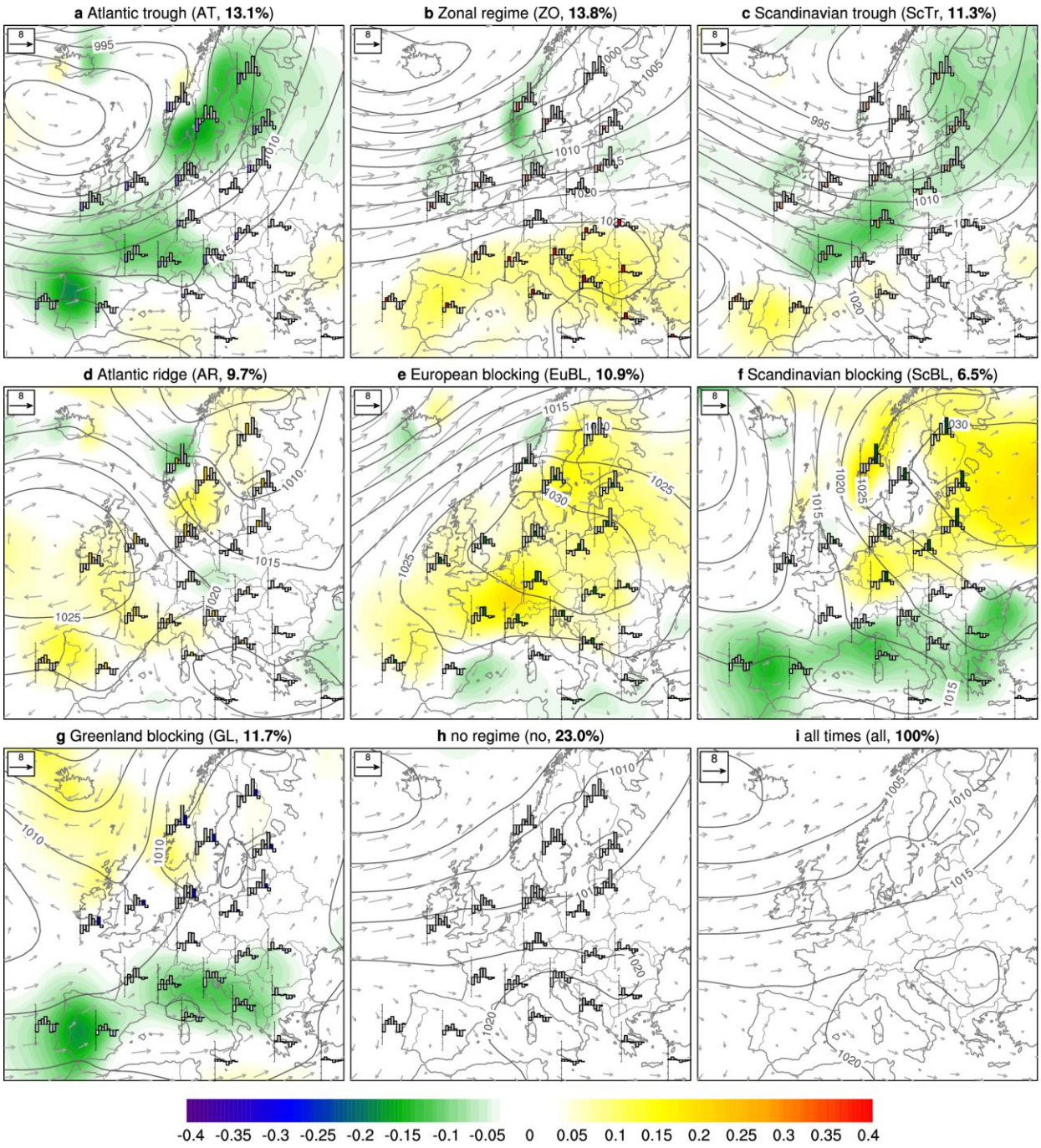

Supplementary Figure 7. Insolation anomalies during the different weather regimes in winter.

As Fig. 2, but anomalies of the daily fraction of insolation and daily potential insolation assuming clear skies (green-yellow shading), absolute wind at about 100 m (grey vectors), and mean sea level pressure (contours every 5 hPa) but for winter days during each regime (a-g), no regime (h), and whole winter (i). Country-specific barplots from Supplementary Fig. 6a, with respective regime coloured. Frequency of weather regimes (%) in panel captions.

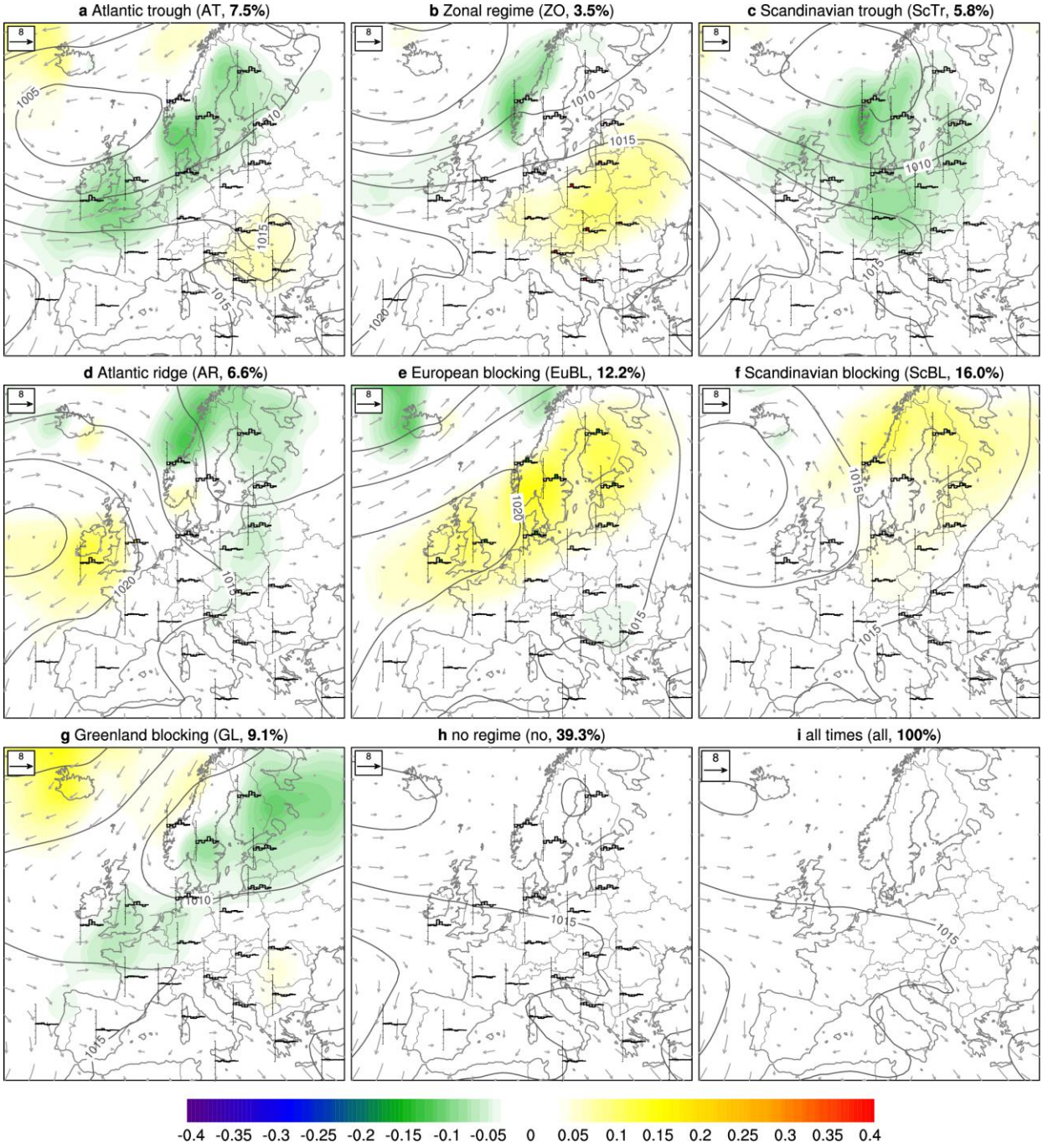

Supplementary Figure 8. Insolation anomalies during the different weather regimes in summer.

As Supplementary Fig. 7, but for summer.

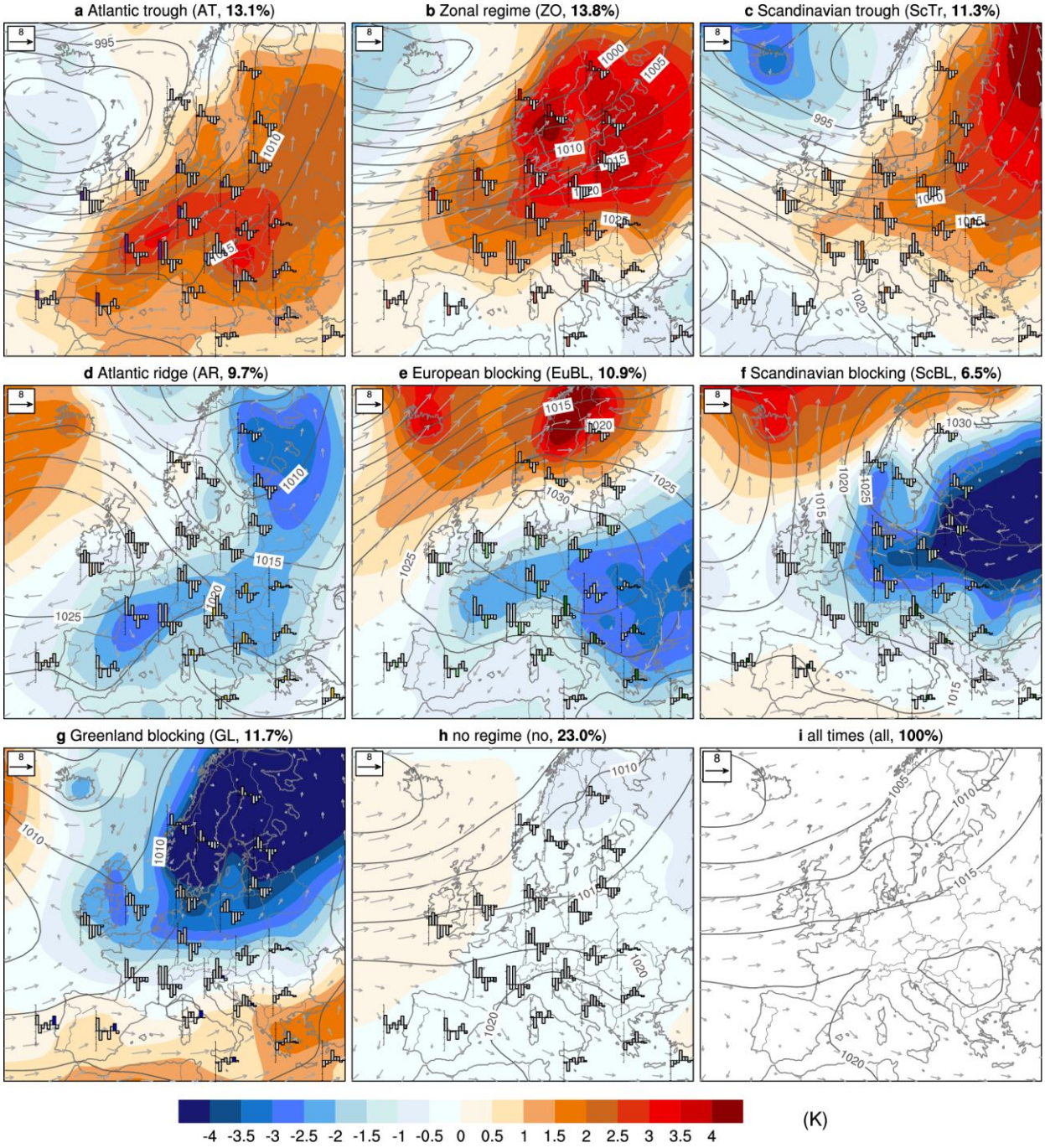

Supplementary Figure 9. 2 m temperature anomalies during the different weather regimes in winter.

As Fig. 2, but anomalies of 2 m temperatures (blue-red shading in K) computed with respect to the 30-day running average at the respective calendar day, absolute wind at about 100 m (grey vectors), and mean sea level pressure (contours every 5 hPa) for winter days during each regime (a-g), no regime (h), and whole summer (i). Country-specific barplots from Supplementary Fig. 4a, with respective regime coloured. Frequency of weather regimes (%) in panel captions.

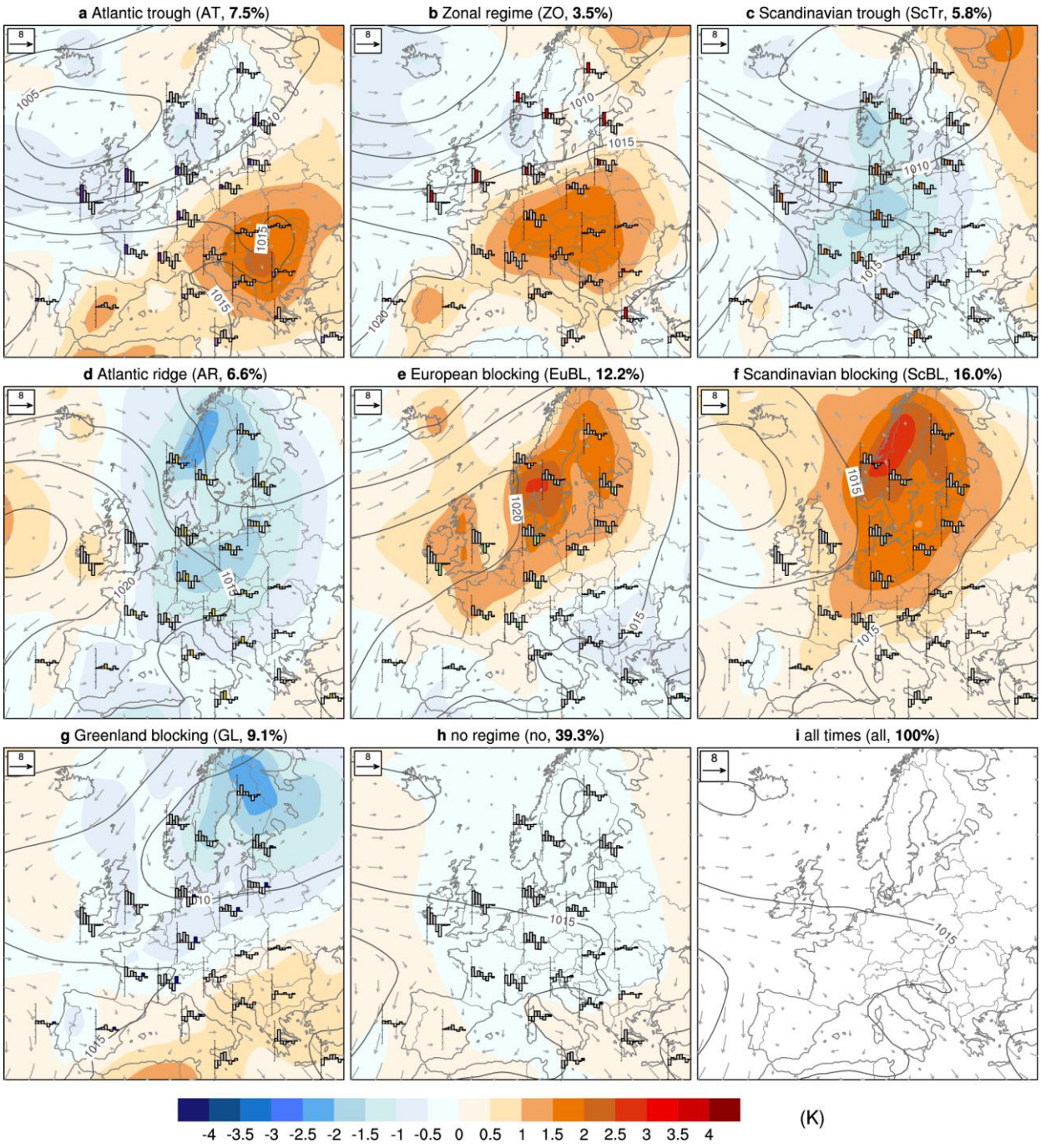

Supplementary Figure 10. 2 m temperature anomalies during the different weather regimes in summer.

As Supplementary Fig. 9, but for summer.

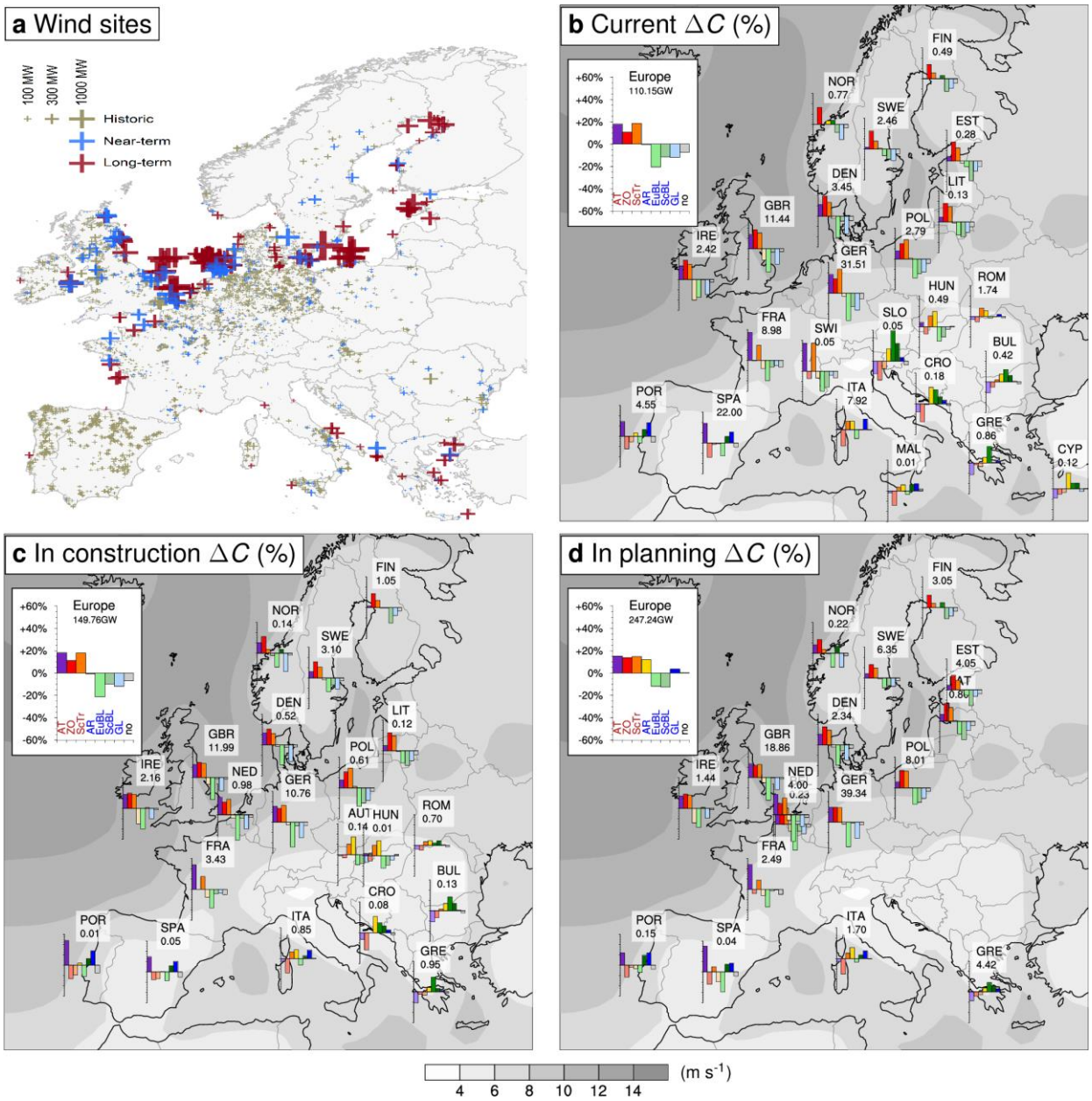

Supplementary Figure 11. Wind sites and relative change in wind generation in winter for the current, near-term/in construction, long-term/in planning wind fleets.

(a) Wind sites adapted from Fig. 3 in Staffell and Pfenninger[23]: Locations and capacities of wind farms modelled for the current, near-term (2020), and long-term (2030) planned wind fleets. (b-d) as Fig. 1 and Supplementary Fig. 3a $\Delta CF_{wr,country}$ in winter (DJF) for available countries based on the current wind fleet as of 2015 (b, "historic", BEL, NED, LUX, LAT, CZE, SVK, AUT omitted for visualisation), only for sites of new wind farms in construction (c, "near-term"), and only for sites of new wind farms in planning (d, "long-term").

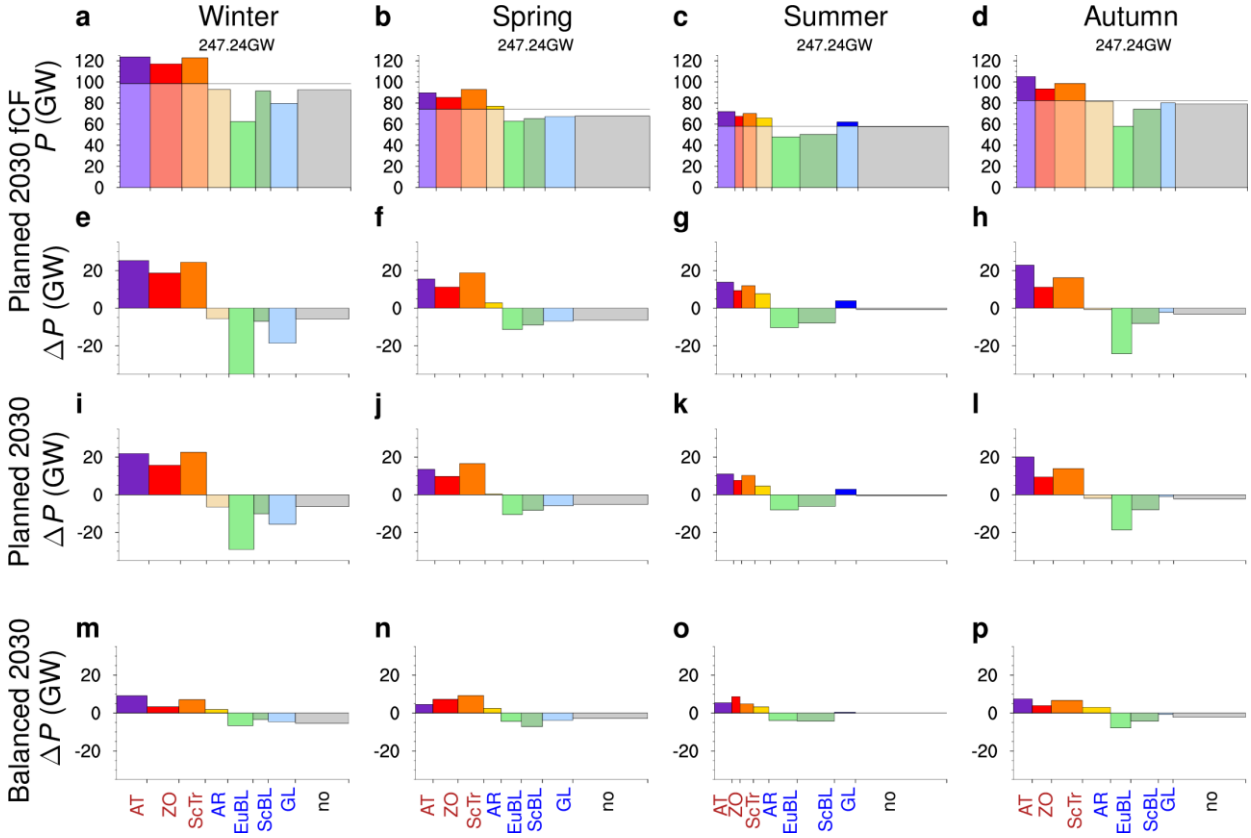

Supplementary Figure 12. Seasonality in future scenarios.

Production (*P*) in GW (a-d) and absolute difference in *P* to seasonal mean (e-h) in GW aggregated for Europe as in Supplementary Fig. 3 but for the "2030 Planned fCF" scenario following current planning and using future *CF*s. (i-p) as Fig. 4e,f absolute difference in *P* to seasonal mean in GW aggregated for Europe but for all seasons. (i-l) "Planned 2030" scenario using constant *CF*s for future deployment following current planning and (m-p) "Balanced 2030" scenario using constant *CF*s for future deployment focussed in Iberia, the Balkans, and northern Scandinavia.

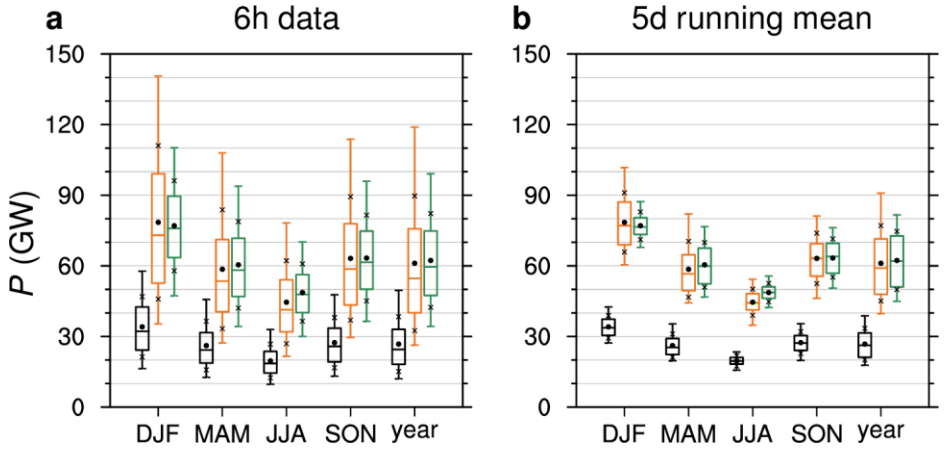

Supplementary Figure 13. Intra-annual volatility of European wind generation.

As Fig. 5b but for all seasons and all year. Box and whisker plots summarising the intra-seasonal variability from 1985-2015 in (a) six-hourly and (b) the 5-day averaged wind generation for the three main scenarios (black: "Current", orange "2030 Planned", green "2030 Balanced"). Box shows the lower and upper quartile and median, whiskers the 5th and 95th percentiles, dot the mean, and crosses the mean ± one standard deviation.

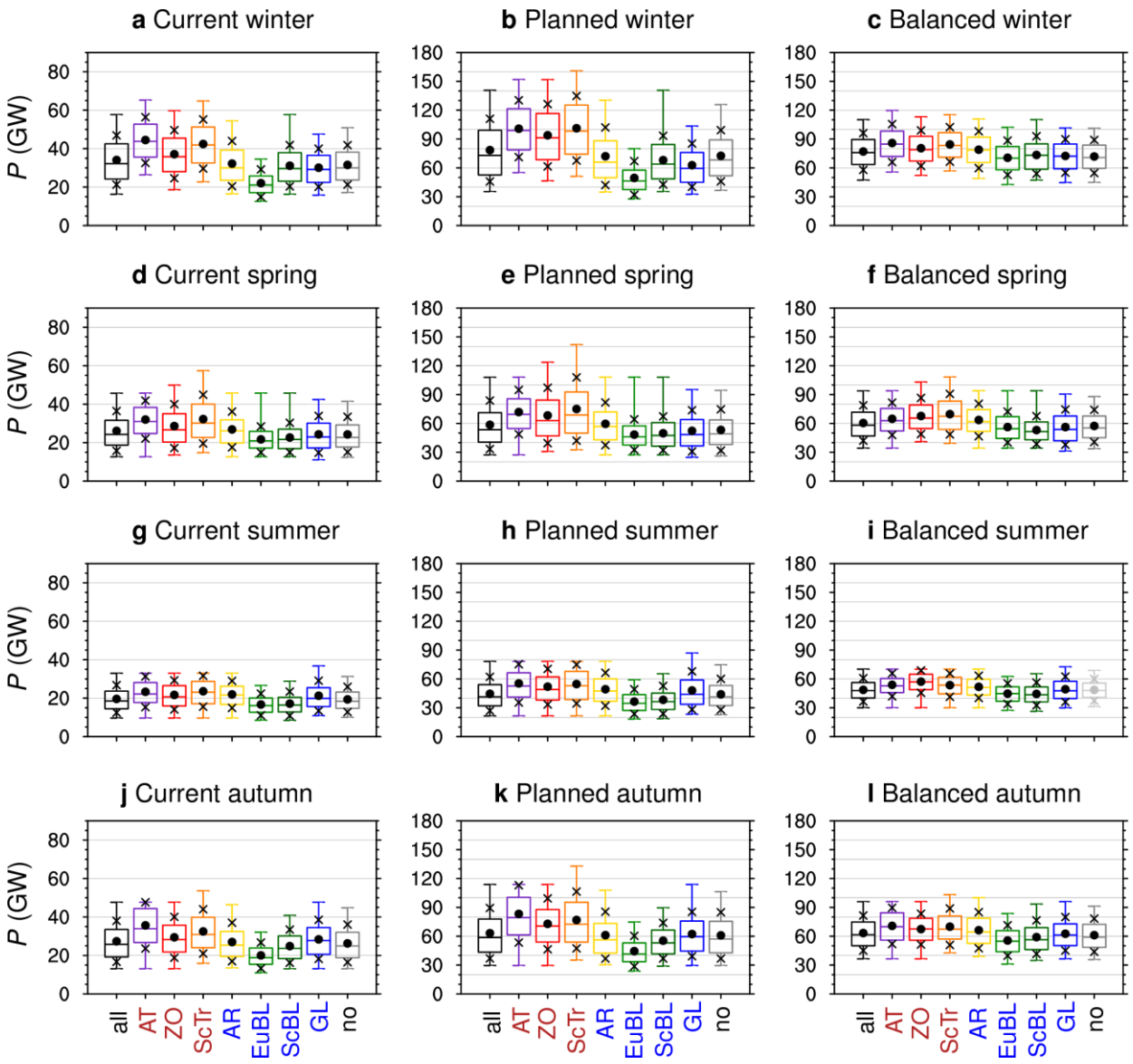

Supplementary Figure 14. Intra-regime volatility of European wind generation.

Box-and-whisker plots show the 5th, 25th, 50th, 75th, 95th percentiles, dots the mean, and crosses the mean ± one standard deviation of total European wind production *P* in GW for the entire season (all), all six-hourly time steps during 1.1.1985-30.6.2016 classified into one of the 7 weather regime, or no regime. Pale colours (only no regime in summer (i)) indicate configurations for that the mean is not significant at the 5% level of a two-sided students t-test. Rows show different seasons, and columns the "Current", "2030 Planned", and "2030 Balanced" scenarios based on current *CF*s, respectively. Note the different scales for the current and future scenarios.

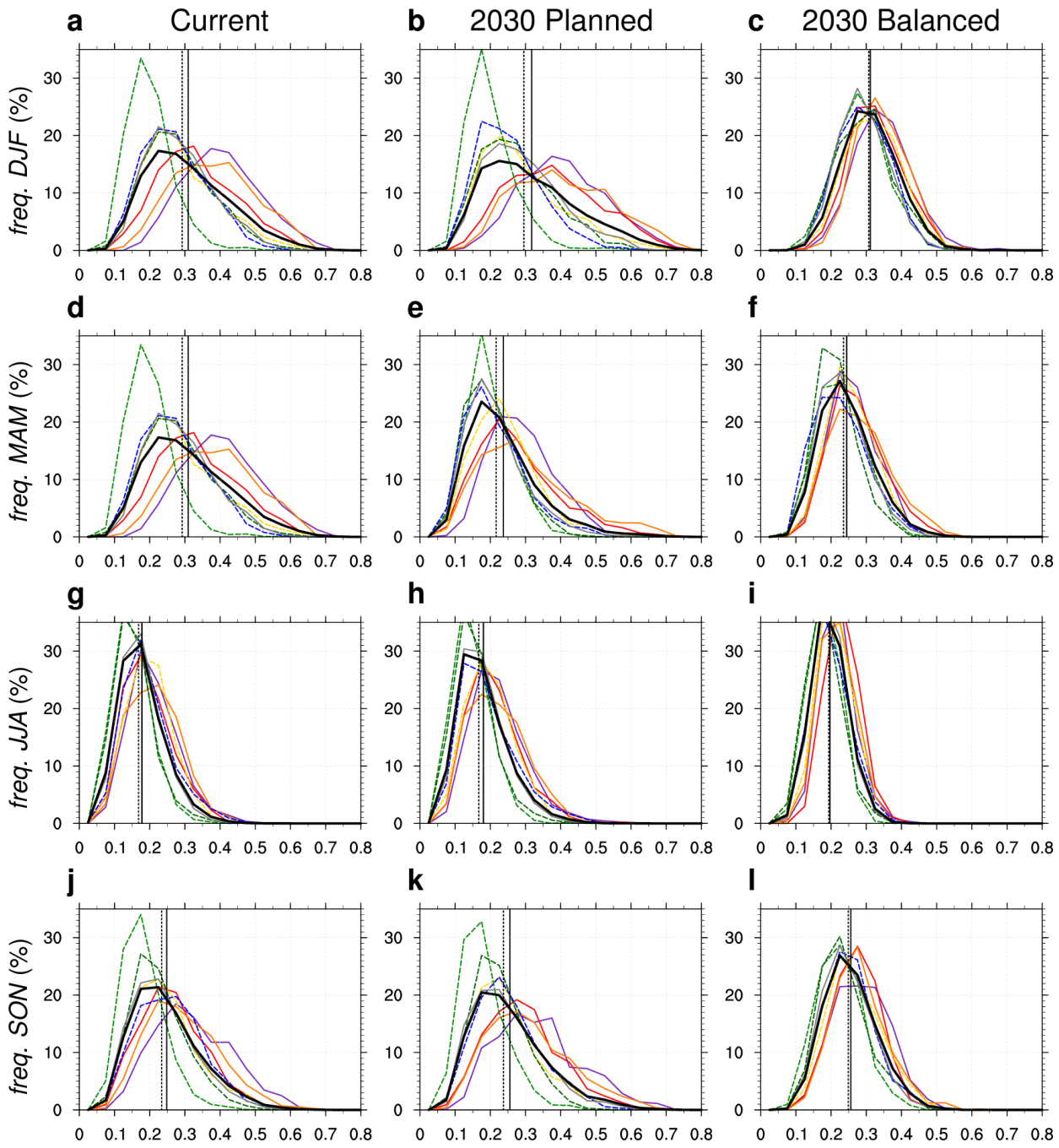

Supplementary Figure 15. Frequency distribution of European wind *CF*.

As Fig. 5c-e but for all seasons. Frequency distribution of European wind capacity factors ($CF^*_{wr,Europe}$) normalised by Europe-wide installed capacity for all six-hourly times from 1985-2015 attributed to a weather regime (colours as in Supplementary Fig. 14), no regime (grey), and all times in the respective season (black). Blocked regimes highlighted with dashed lines. Bin width is 0.05. The vertical black dashed (solid) line shows the median (mean) for all times. In contrast to Fig. 1 (inset) and Fig. 3a, $CF^*_{wr,Europe}$ is here simply weighted by Europe-wide installed capacity, to reflect the actual production in Europe's wind fleet rather than its hypothetical production potential (see Methods). (a-c) winter, (d-f) spring, (g-i) summer, (j-l) autumn; (a,d,g,j) current system, (b,e,h,k) "2030 Planned" scenario, (c,f,i,l) "2030 Balanced" scenario.

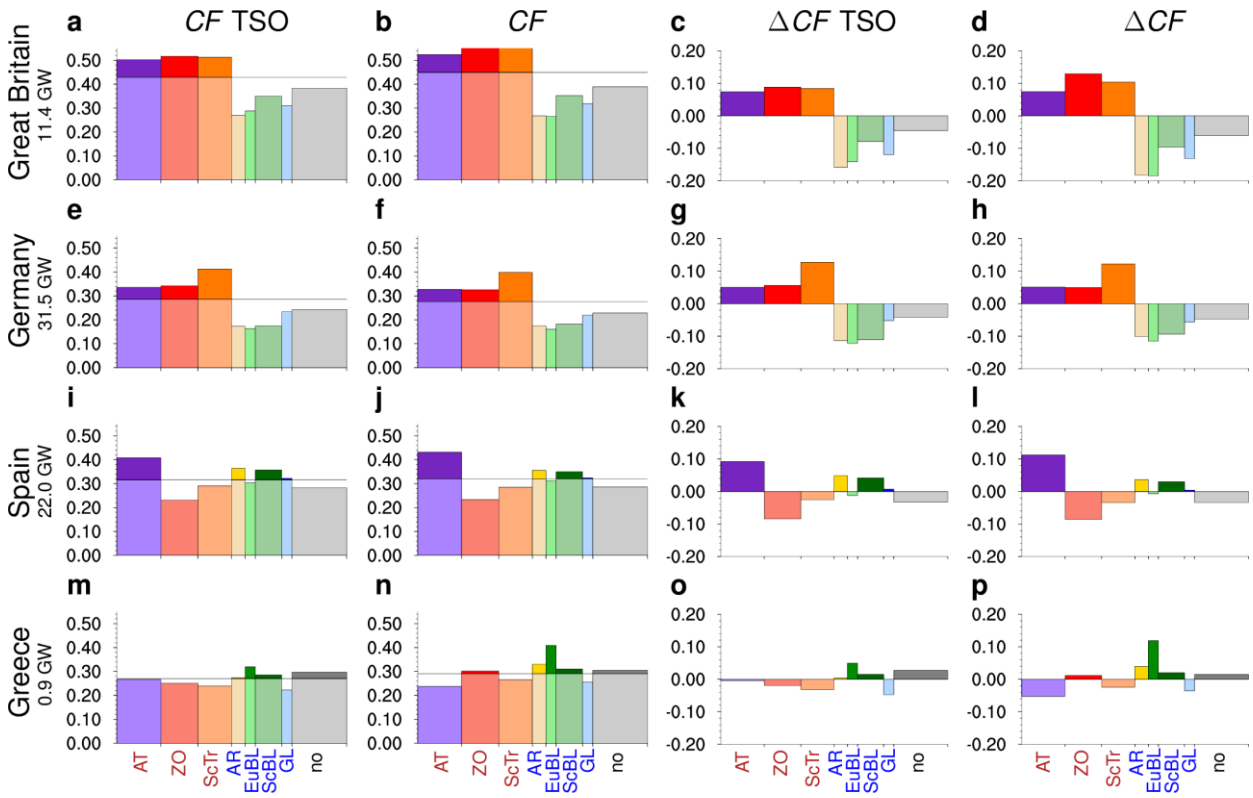

Supplementary Figure 16. Wind capacity factors based on operator data for selected countries in winter.

Wind *CF* for selected countries (rows) based on TSO data (1st column; Supplementary Table 7) and from Renewables.ninja (2nd column) during the seven regimes and no regime in winter. The horizontal line indicates winter mean *CF*, bars are coloured dark above, light coloured below. Difference in wind capacity factors *ΔCF* to winter mean based on TSO data (3rd column) and from Renewables.ninja (4th column). Data is shown for December, January, February during 01.01.2011 to 29.02.2016 only and bars are scaled according to regime frequencies in that sub-period. Country's installed capacity is indicated in row labels.

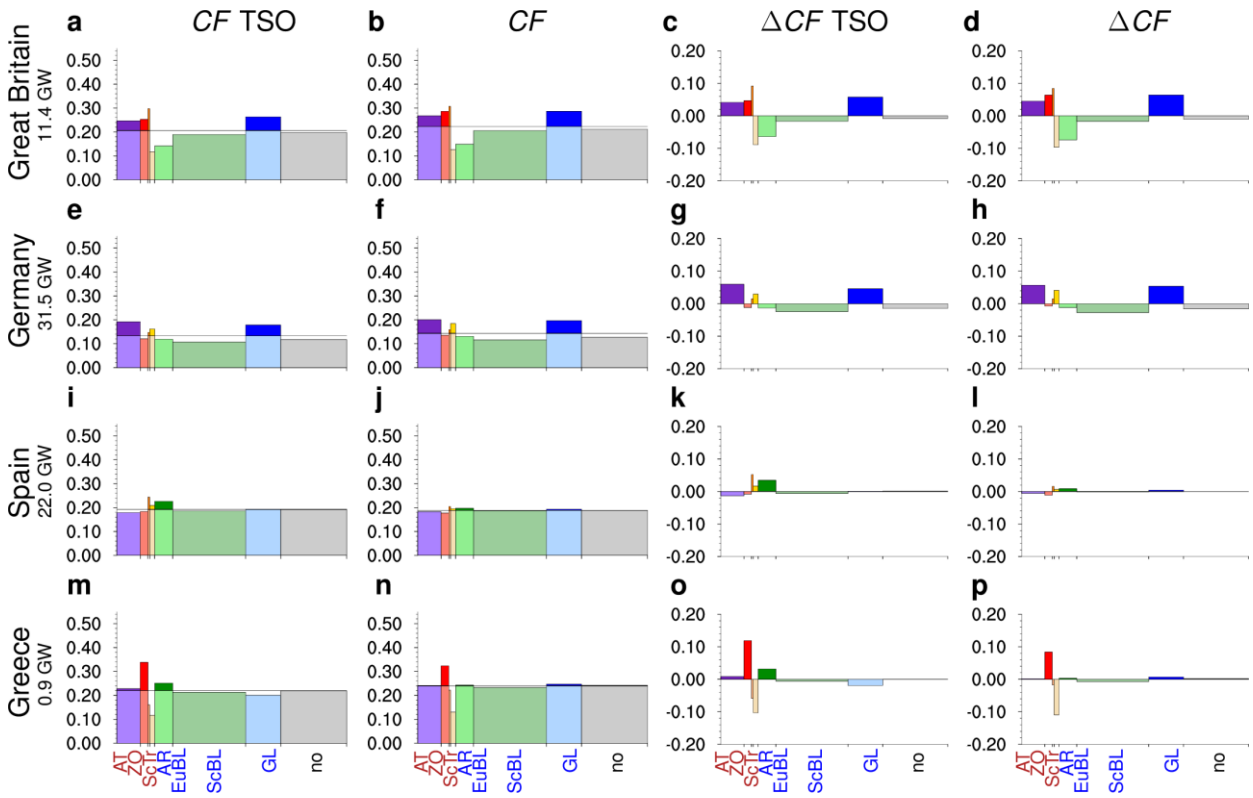

Supplementary Figure 17. Wind capacity factors based on operator data for selected countries in summer.

As Supplementary Fig. 16 but for June, July, August during 01.06.2011 to 31.08.2015.

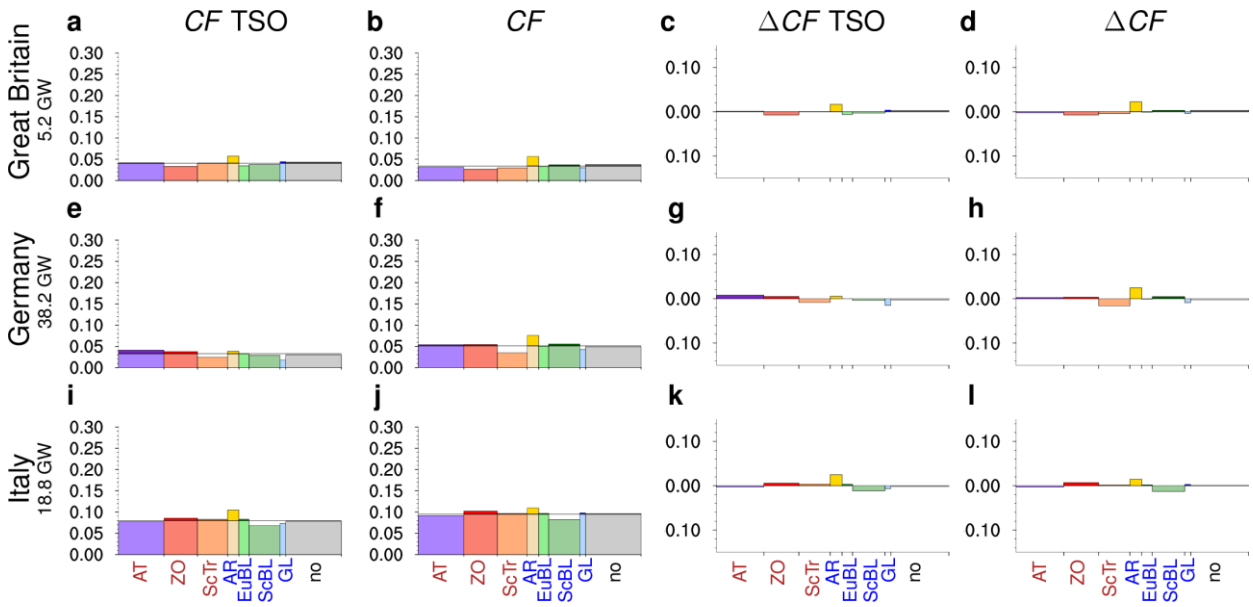

Supplementary Figure 18. Solar PV capacity factors based on operator data for selected countries in winter.

As Supplementary Fig. 16 but capacity factors for solar PV in Great Britain, Germany, and Italy. Data is shown for December, January, February during 01.01.2012 to 29.02.2016 only.

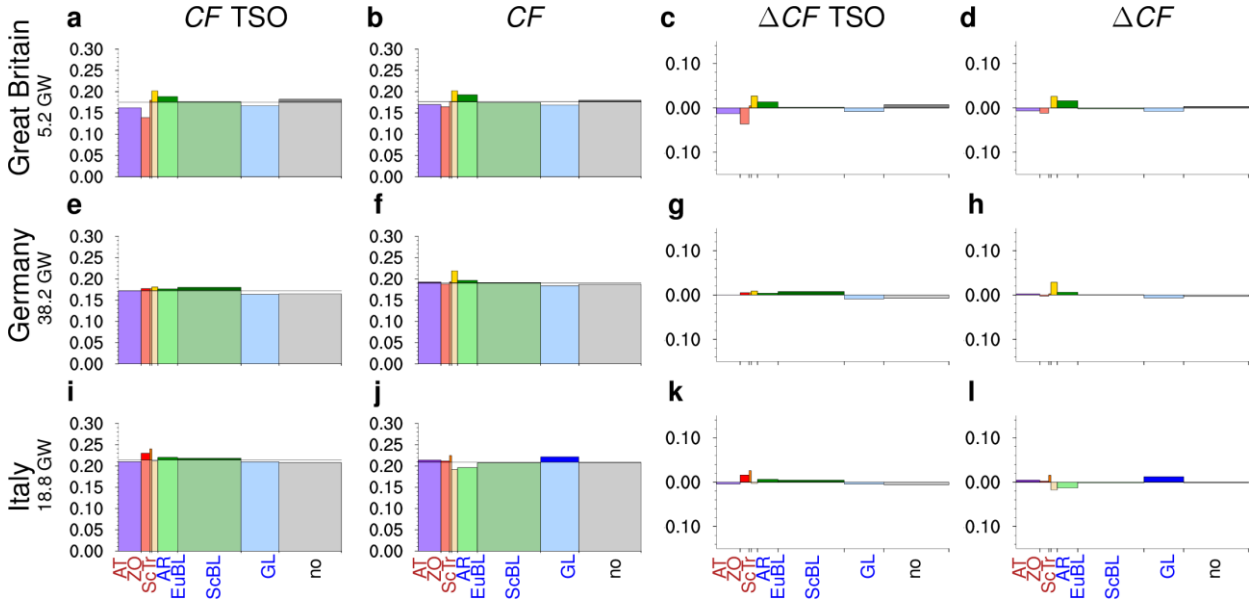

Supplementary Figure 19. Solar PV capacity factors based on operator data for selected countries in summer.

As Supplementary Fig. 18 but for June, July, August during 01.06.2012 to 31.08.2015.

Supplementary Table 1. Mean NAO index during the seven weather regimes and seasonal frequencies.

Top: Mean NAO index during the seven weather regimes in different seasons. See Methods for details of computation. Bottom: Seasonal frequencies in percent.

season	**AT**	**ZO**	**ScTr**	**AR**	**EuBL**	**ScBL**	**GL**	**no**
DJF	+0.40	+0.99	+0.88	-0.22	+0.26	-0.18	-0.84	+0.23
MAM	-0.04	+1.02	+0.60	-0.20	+0.65	0.01	-0.93	+0.13
JJA	-0.51	+0.83	+0.43	-0.19	+0.70	-0.36	-1.31	+0.00
SON	-0.35	+0.88	+0.19	-0.36	+0.66	-0.33	-1.52	-0.03
DJF	13.1%	13.8%	11.3%	9.75	10.9%	6.5%	11.7%	23.0%
MAM	7.5%	10.8%	11.0%	7.55	8.7%	9.1%	13.1%	32.3%
JJA	7.5%	3.5%	5.8%	6.6%	12.2%	16.0%	9.1%	39.3%
SON	8.0%	8.3%	13.3%	12.1%	8.7%	11.9%	6.3%	31.3%

Supplementary Table 2. Wind power scenarios.

Name and characteristics of the different wind power generation scenarios. Different capacity factors and installed capacities are used as provided by the "historic, near-term, long-term" scenarios from Renewables.ninja data[23].

Scenario name	***Information***
Current	Basic scenario using installed capacity and country-specific current *CF*s based on technology and sites of wind farms as of 2015.
2030 Planned	Conservative future scenario using country-specific **current *CF*s** based on technology and sites of wind farms as of 2015 for a Europe-wide total of 137.094 GW of newly installed capacity until 2030 distributed according to current planning.
2030 Balanced	Conservative balanced future scenario using country-specific **current *CF*s** based on technology and sites of wind farms as of 2015 for in total 137.000 GW of newly installed capacity in **Iberia**: 25 GW in Portugal, 5 GW in Spain, in **Scandinavia**: 20 GW in Norway, 20 GW in Finland, and in the **Balkans**: 42 GW in Greece, 10 GW in Bulgaria, 10 GW in Croatia, and 5 GW in Slovenia.
2030 Balanced simple	Simpler balanced future scenario using country-specific **current *CF*s** based on technology and sites of wind farms as of 2015 with new deployment only in **Portugal** (+30 GW)**, Finland** (+40 GW), and **Greece** (+67 GW). For comparison with scenario "2030 Balanced simple fCF"
2030 Planned fCF	Future scenario using current *CF* with installed capacity as of 2015, near-term future *CF* for new wind farms (39.613 GW) currently under construction and expected online by 2020, and long-term future *CF* with 97.481 GW of currently planned capacity expected to be online by 2030 according to current planning.
2030 Balanced simple fCF	As "2030 Balanced simple" but using current *CF* with installed capacity as of 2015, near-term future *CF* for Greece with 40.094 GW newly installed capacity online by 2020, and long-term future *CF* for newly installed capacity between by 2030 in Portugal (+30 GW), Finland (+40 GW), and Greece (27 GW).

Supplementary Table 3. Wind power output in the "Current" system.

Absolute mean electricity generation, volatility, and deviation from the mean in generation for the regime with minimum and maximum mean power output in all seasons for the current installed capacities (as of 2015 wind 110.15 GW, solar PV 87.91 GW) and aggregated over Europe.

Current	***P* [GW]**	**volatility [GW]**	**minimum *P* [GW]**	**maximum *P* [GW]**
wind DJF	33.91	22.45	EuBL -12.12	AT +10.33
wind MAM	26.38	10.72	EuBL -4.55	ScTr +6.17
wind JJA	20.02	6.90	EuBL -2.89	ScTr +4.00
wind SON	27.21	15.62	EuBL -7.37	AT +8.25
pv DJF	6.01	1.91	AT -0.84	EuBL +1.07
pv MAM	14.65	2.59	ScTr -1.23	EuBL +1.36
pv JJA	17.34	0.88	GL -0.35	ZO +0.54
pv SON	9.60	2.28	ZO -1.14	EuBL +1.14

Supplementary Table 4. Wind power output in the "2030 Planned" scenarios.

As Supplementary Table 3 but for the "2030 Planned" (247.24 GW) scenario using current *CF*s (top) and future *CF*s (bottom) and only wind power.

2030 Planned	***P* [GW]**	**volatility [GW]**	**minimum *P* [GW]**	**maximum *P* [GW]**
wind DJF	78.18	51.68	EuBL -29.08	ScTr +22.60
wind MAM	58.92	27.10	EuBL -10.51	ScTr +16.59
wind JJA	45.43	19.13	EuBL -8.08	AT +11.04
wind SON	62.84	38.76	EuBL -18.68	AT +20.08
wind DJF	98.43	61.27	EuBL -35.98	AT +25.29
wind MAM	74.15	30.13	EuBL -11.31	ScTr +18.81
wind JJA	58.15	24.12	EuBL -10.32	AT +13.80
wind SON	82.31	47.05	EuBL -24.18	AT +22.86

Supplementary Table 5. Wind power output in the "2030 Balanced" scenario.

As Supplementary Table 3 but for the "2030 Balanced" scenario (247.15 GW) with new capacity installed in Iberia, the Balkans, and northern Scandinavia and using current *CF*s.

2030 Balanced	***P* [GW]**	**volatility [GW]**	**minimum *P* [GW]**	**maximum *P* [GW]**
wind DJF	76.65	15.71	EuBL -6.59	AT +9.12
wind MAM	60.72	16.42	ScBL -7.13	ScTr +9.29
wind JJA	49.09	12.97	ScBL -4.26	ZO +8.71
wind SON	63.07	15.33	EuBL -7.86	AT +7.47

Supplementary Table 6. Wind power output in the "2030 Balanced simple" scenarios.

As Supplementary Table 3 but for the balanced "2030 Balanced simple" scenarios (247.15 GW) with new capacity installed only in Portugal, Greece, and Finland using current *CF*s (top) and future *CF*s (bottom).

2030 Balanced simple	***P* [GW]**	**volatility [GW]**	**minimum *P* [GW]**	**maximum *P* [GW]**
wind DJF	76.70	14.61	EuBL -6.09	AT +8.51
wind MAM	61.51	15.95	ScBL -7.34	ScTr +8.61
wind JJA	52.39	15.23	EuBL -4.32	ZO +10.91
wind SON	63.91	14.72	EuBL -8.01	AT +6.71
wind DJF	96.73	13.74	no -5.64	AT +8.10
wind MAM	80.23	16.36	ScBL -7.31	ScTr +9.05
wind JJA	70.09	20.61	EuBL -5.37	ZO +15.24
wind SON	83.11	15.30	EuBL -8.93	ZO +6.37

Supplementary Table 7. Operator data.

Availability of hourly capacity factors derived from TSO-reported power output.

Country	**Wind**	**PV**	**Source**
France	1.1.2011-30.5.2016	1.1.2012-30.5.2016	RTE[a]
Germany	1.1.2010-30.5.2016	1.1.2012-30.5.2016	OPSD[b]
Greece	1.1.2009-30.5.2016	n/a	AΔMHE[c]
Italy	1.1.2011-30.5.2016	1.1.2011-30.5.2016	Terna[d]
Spain	1.1.2009-30.5.2016	1.1.2015-30.5.2016	REE[e]
Sweden	1.1.2007-30.5.2016	n/a	SVK[f]
United Kingdom	1.1.2009-30.5.2016	1.1.2012-30.5.2016	Elexon[g] and National Grid[h]
Overlap period used	**1.1.2011-30.5.2016**	**1.1.2012-30.5.2016**	

Supplementary Database 1. Mean capacity factors.

Each file <type>_<season>.txt contains an ASCII table as detailed in the following. Here <type> is "pv" for the scenario of current solar PV installations in each country as of 2015, "wind_current" for current wind installations as of 2015, "wind_nearterm" for new wind installations until 2020, and "wind_longterm" for new wind installations between 2020-2030.

The columns in each file contain the 3 letter ISO code of a country, the area in km^2, the installed capacity *IC* in GW, and the mean capacity factor $CF_{wr,country,season}$ of all days of a season, and all days attributed to one of the seven weather regimes or to no regime. Note that for "wind_nearterm" and "wind_longterm" $CF_{wr,country,season}$ is the capacity factor only valid for the fraction of newly installed capacity in the respective time periods and it accounts for an increase in offshore deployment and technical innovation.

[a] http://www.rte-france.com/en/eco2mix/eco2mix-telechargement-en
[b] http://data.open-power-system-data.org/time_series/
[c] http://www.admie.gr/leitoyrgia-dedomena/leitoyrgia-agoras-ilektrikis-energeias/agora-diacheirisis-isozygioy-ischyos/dedomena-eisodoy/
[d] http://www.terna.it/it-it/sistemaelettrico/transparencyreport/generation/expostdataontheactualgeneration.aspx
[e] https://demanda.ree.es/movil/peninsula/demanda/total
[f] http://www.svk.se/aktorsportalen/elmarknad/statistik
[g] https://www.elexonportal.co.uk/fuelhh
[h] http://www2.nationalgrid.com/UK/Industry-information/Electricity-transmission-operational-data/Data-Explorer/